Lysophosphatidic Acid-Mediated GPR35 Signaling in CX3CR1+ Macrophages Regulates Intestinal Homeostasis

Berna Kaya, Cristian Doñas, Philipp Wuggenig, Oscar E Diaz, Rodrigo A Morales, Hassan Melhem, Pedro P Hernández, Tanay Kaymak, Srustidhar Das, Petr Hruz, et al.

Cell Reports

Article

Lysophosphatidic Acid-Mediated GPR35 Signaling in CX3CR1^{+} Macrophages Regulates Intestinal Homeostasis

Graphical Abstract

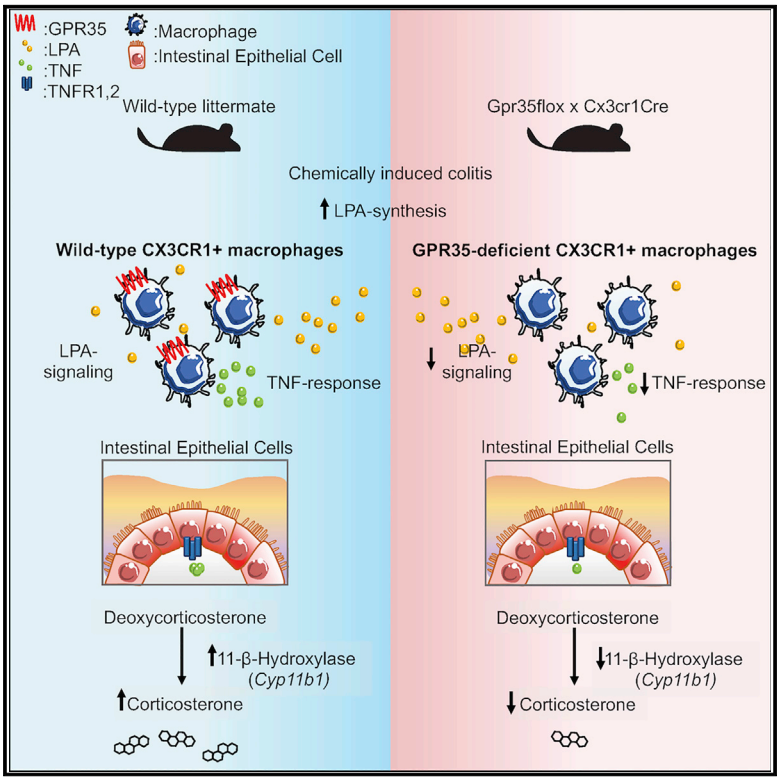

Highlights

- Inflammatory cues and the microbiota modulate *Gpr35* expression across species
- LPA modulates GPR35-dependent functions in zebrafish and mouse macrophages
- GPR35-expressing macrophages have a protective role during intestinal inflammation
- GPR35 controls intestinal inflammation by inducing TNF and corticosterone synthesis

Authors

Berna Kaya, Cristian Doñas, Philipp Wuggenig, ..., C. Korcan Ayata, Eduardo J. Villablanca, Jan Hendrik Niess

Correspondence

eduardo.villablanca@ki.se (E.J.V.), janhendrik.niess@unibas.ch (J.H.N.)

In Brief

GPR35 is associated with IBD, but how GPR35 may influence macrophage-mediated intestinal homeostasis remains unclear. Using zebrafish and mice genetic tools, Kaya and colleagues have identified that LPA triggers GPR35 activity and that loss of macrophage GPR35 signaling confers intrinsic dysfunctions with effects on cytokine production and intestinal homeostasis.

Kaya et al., 2020, Cell Reports *32*, 107979
August 4, 2020
https://doi.org/10.1016/j.celrep.2020.107979

CellPress

Cell Reports

CellPress
OPEN ACCESS

Article

Lysophosphatidic Acid-Mediated GPR35 Signaling in CX3CR1^{+} Macrophages Regulates Intestinal Homeostasis

Berna Kaya,[1] Cristian Doñas,[2,3] Philipp Wuggenig,[1] Oscar E. Diaz,[2,3] Rodrigo A. Morales,[2,3] Hassan Melhem,[1] Swiss IBD. Cohort Investigators, Pedro P. Hernández,[4] Tanay Kaymak,[1] Srustidhar Das,[2,3] Petr Hruz,[5] Yannick Franc,[6] Florian Geier,[1,7] C. Korcan Ayata,[1] Eduardo J. Villablanca,[2,3,8,9,*] and Jan Hendrik Niess[1,5,8,*]

[1]Department of Biomedicine, University of Basel, 4031 Basel, Switzerland
[2]Division of Immunology and Allergy, Department of Medicine, Solna, Karolinska Institutet and University Hospital, 17176 Stockholm, Sweden
[3]Center for Molecular Medicine (CMM), 17176 Stockholm, Sweden
[4]Institut Curie, PSL Research University, INSERM U934/CNRS UMR3215, Development and Homeostasis of Mucosal Tissues Group, 75005 Paris, France
[5]University Center for Gastrointestinal and Liver Diseases, St. Clara Hospital and University Hospital of Basel, 4031 Basel, Switzerland
[6]Center for Primary Care and Public Health (Unisanté), University of Lausanne, 1011 Lausanne, Switzerland
[7]Swiss Institute of Bioinformatics, 4031 Basel, Switzerland
[8]These authors contributed equally
[9]Lead Contact
*Correspondence: eduardo.villablanca@ki.se (E.J.V.), janhendrik.niess@unibas.ch (J.H.N.)
https://doi.org/10.1016/j.celrep.2020.107979

SUMMARY

Single-nucleotide polymorphisms in the gene encoding G protein-coupled receptor 35 (GPR35) are associated with increased risk of inflammatory bowel disease. However, the mechanisms by which GPR35 modulates intestinal immune homeostasis remain undefined. Here, integrating zebrafish and mouse experimental models, we demonstrate that intestinal *Gpr35* expression is microbiota dependent and enhanced upon inflammation. Moreover, murine GPR35^{+} colonic macrophages are characterized by enhanced production of pro-inflammatory cytokines. We identify lysophosphatidic acid (LPA) as a potential endogenous ligand produced during intestinal inflammation, acting through GPR35 to induce tumor necrosis factor (*Tnf*) expression in macrophages. Mice lacking *Gpr35* in CX3CR1^{+} macrophages aggravate colitis when exposed to dextran sodium sulfate, which is associated with decreased transcript levels of the corticosterone-generating gene *Cyp11b1* and macrophage-derived *Tnf* . Administration of TNF in these mice restores *Cyp11b1* expression and intestinal corticosterone production and ameliorates DSS-induced colitis. Our findings indicate that LPA signals through GPR35 in CX3CR1^{+} macrophages to maintain TNF-mediated intestinal homeostasis.

INTRODUCTION

Genome-wide association studies (GWASs) have identified single-nucleotide polymorphisms in *GPR35* that are associated with increased risk of ulcerative colitis (UC) (Ellinghaus et al., 2013; Imielinski et al., 2009). Structural modeling studies have suggested that protein-coding variant rs3749171, which leads to the T108M substitution, may affect GPR35 activation (Ellinghaus et al., 2013); however, how defective GPR35 signaling influences intestinal immune homeostasis is poorly understood. The endogenous ligand for GPR35 also remains undefined, although the chemokine CXCL17, the tryptophan metabolite kynurenic acid (KYNA), and the phospholipid derivative lysophosphatidic acid (LPA) have been suggested as putative ligands (Maravillas-Montero et al., 2015; Oka et al., 2010; Wang et al., 2006). Studies have suggested that specific ligands might activate GPR35 in a context- and species-dependent manner. CXCL17 did not activate migration of GPR35-expressing cells in one study (Binti Mohd Amir et al., 2018); KYNA has a wide spectrum of potency for GPR35 across species, with low potency in humans (Mackenzie et al., 2011); and LPA has not been experimentally pursued as a potential GPR35 ligand following the initial suggestion of its role in elevating intracellular Ca(2+) and inducing receptor internalization (Oka et al., 2010). Thus, the putative GPR35 ligand that might control immune responses *in vivo* remains to be identified.

GPR35 is highly expressed in the intestinal epithelial cells (IECs) and macrophages in both humans and mice (Lattin et al., 2008), and activation of GPR35 promotes IEC turnover during wound healing (Schneditz et al., 2019; Tsukahara et al., 2017). Kaneider and colleagues have recently shown that *Gpr35* deficiency results in decreased inflammation-associated intestinal tumorigenesis (Schneditz et al., 2019). In addition, Gpr35$^{-/-}$ IECs have reduced turnover compared to control mice (Schneditz et al., 2019; Tsukahara et al., 2017). In agreement with a role in IEC turnover, GPR35 is protective during

chemically induced acute colonic inflammation in mice (Farooq et al., 2018).

Several lines of evidence have implicated intestinal CX3CR1$^+$ macrophages in inflammatory bowel disease (IBD) (Bernardo et al., 2018; Imielinski et al., 2009). The critical role of macrophages in the intestine has been demonstrated by targeted depletion of tolerogenic signals in CX3CR1$^+$ macrophages (Bernshtein et al., 2019; Shouval et al., 2014; Zigmond et al., 2014). In addition, CX3CR1$^+$ macrophages are also part of the inflammatory cell infiltrates in colitic mice and IBD patients (MacDonald et al., 2011). GPR35 is expressed in bone-marrow-derived macrophages (BMDMs) and peritoneal macrophages, and it modulates the activity of Na/K-ATPase to control macrophage metabolism (Schneditz et al., 2019; Tsukahara et al., 2017). However, whether GPR35 signaling in macrophages is critical to establish intestinal immune homeostasis *in vivo* and the putative ligand that may trigger GPR35-dependent functions in macrophages are yet to be understood.

Anti-TNF (tumor necrosis factor) antibodies have been successfully implemented in the clinic for the treatment of IBD (Hanauer et al., 2002; Targan et al., 1997). Inhibition of TNF also prevents symptoms in mouse models, including spontaneous ileitis (Günther et al., 2011), 2,4,6-trinitrobenzenesulfonic acid (TNBS) colitis (Neurath et al., 1997), and transfer colitis (Corazza et al., 1999). Besides the well-described pro-inflammatory role of TNF in colitis, some evidence suggests anti-inflammatory functions. For example, in the dextran sodium sulfate (DSS) colitis model, in which intestinal inflammation is achieved upon disruption of the mucosal barrier integrity (Wirtz et al., 2007), the neutralization or deficiency of TNF lead to exacerbation of colitis (Naito et al., 2003). This has been attributed to TNF-mediated induction of apoptosis in T cells and regulation of extra-adrenal corticosterone production by IEC, which, in turn, may suppress immune responses (Naito et al., 2003).

Here, we report that high *Gpr35* expression in the gastrointestinal tract is conserved across species. Using *in vitro* and *in vivo* approaches in *gpr35* mutant zebrafish, *Gpr35*-deficient mice, and cells expressing human GPR35, we identify LPA as a potential endogenous ligand that triggers GPR35-dependent induction of TNF production by macrophages. Conditional deletion of *Gpr35* in CX3CR1$^+$ macrophages in mice results in increased susceptibility to DSS-induced colitis, associated with reduced TNF production and *Cyp11b1* expression. Finally, TNF administration to mice lacking *Gpr35* in macrophages correlated with attenuated DSS-induced colitis and restored *Cyp11b1* expression. Thus, our data indicate that LPA-mediated GPR35 activation controls TNF production and ameliorates intestinal inflammation.

RESULTS

Colonic Macrophages Express GPR35

Our interest in using zebrafish (*Danio rerio*) to investigate the function of IBD-associated risk genes led us to clone and characterize the functional zebrafish homolog of *GPR35*. We identified two *GPR35* paralogs in zebrafish, *gpr35a* and *gpr35b*, which share 25.6% and 24% identity, respectively, with the human GPR35 protein sequence (Figure S1A). Of note, *gpr35a* and *gpr35b* were more closely related phylogenetically to human *GPR35* and murine *Gpr35* than to human or murine *GPR55*, a highly similar gene (Figure S1B). Gene expression analysis revealed that, by 120 h post-fertilization (hpf), *gpr35a* expression was comparable between the intestine and the rest of the body, whereas *gpr35b* was predominantly expressed in the intestine (Figures 1A and S1C). This finding was confirmed by whole-mount *in situ* hybridization (WISH), which showed expression of *gpr35b* specifically in the intestinal bulb at 120 hpf (Figure 1B). These observations were echoed in our analysis of the human protein atlas (www.proteinatlas.org), which showed the highest *GPR35* transcript levels in the gastrointestinal tract compared to other tissues (Figure S1D). Similarly, qPCR of mouse tissues revealed an increased expression pattern of *Gpr35* from the duodenum to the distal colon, in the proximal stomach, mesenteric lymph nodes (MLNs), and Peyer's patches, compared to other tissues, such as the liver (Figure 1C).

To define the cells expressing GPR35, we generated a *Gpr35*-tdTomato reporter mouse line (Figure S1E). Immunofluorescent staining for GPR35 showed colocalization with tdTomato, indicating that the reporter monitored endogenous *Gpr35* expression (Figure S1F). *Ex vivo* imaging of small and large intestinal tissues from *Gpr35*-tdTomato mice crossed to *Cx3cr1*-GFP reporter mice revealed GPR35 in IECs and lamina propria (LP) CX3CR1$^+$ phagocytes (Figure 1D). In addition, GPR35$^+$ cells were located in the subcapsular sinus and T cell zones of MLNs, in isolated lymph follicles (ILFs), and in the subepithelial dome regions of Peyer's patches, but not in the B cell follicles of MLNs or Peyer's patches (Figure 1D). We observed GPR35 also in CD64$^-$CD11c$^+$ dendritic cells, but not in B cells; CD4$^+$ or CD8$^+$ T cells; neutrophils; natural killer (NK) cells; or innate lymphoid cells, including ILC1, ILC2, and ILC3 (Figure S1G).

CX3CR1$^+$ macrophages derive from blood Ly6C^{high} monocytes that extravasate into the LP, downregulate Ly6C, and develop into mature macrophages through intermediates in a "monocyte waterfall" development (Bain et al., 2013; Wuggenig et al., 2020). Flow cytometry analysis of GPR35 expression during macrophage developmental stages (Steinert et al., 2017) (Figure S1H) revealed that most Ly6C^{high} monocytes in the small intestinal or colonic LP expressed GPR35 (Figure 1E). Percentages of GPR35$^+$ cells gradually decreased to approximately 30% and 50% alongside the differentiation of monocytes into mature macrophages in the small and large intestine, respectively (Figure 1F), suggesting that monocytes downregulate GPR35 toward their differentiation into intestinal macrophages.

To gain insight into the potential function of GPR35$^+$ macrophages, we performed bulk RNA-sequencing (RNA-seq) analysis on sorted GPR35$^-$ and GPR35$^+$ macrophages from the colonic LP. Unsupervised hierarchical clustering and principal-component analysis (PCA) revealed that GPR35$^-$ and GPR35$^+$ macrophages are transcriptionally distinct populations (Figures 1G and S1I), in which GPR35$^+$ macrophages showed higher *Il1b*, *Il1a*, *Tnf*, *Il12b*, and *Il23a* transcripts compared to GPR35$^-$ macrophages (Figure 1H). Taken together, these data show that GPR35 is highly expressed in intestinal tissues across species and that GPR35$^+$ murine colonic macrophages are characterized by higher expression of pro-inflammatory genes than the GPR35$^-$ counterpart.

CellPress
OPEN ACCESS

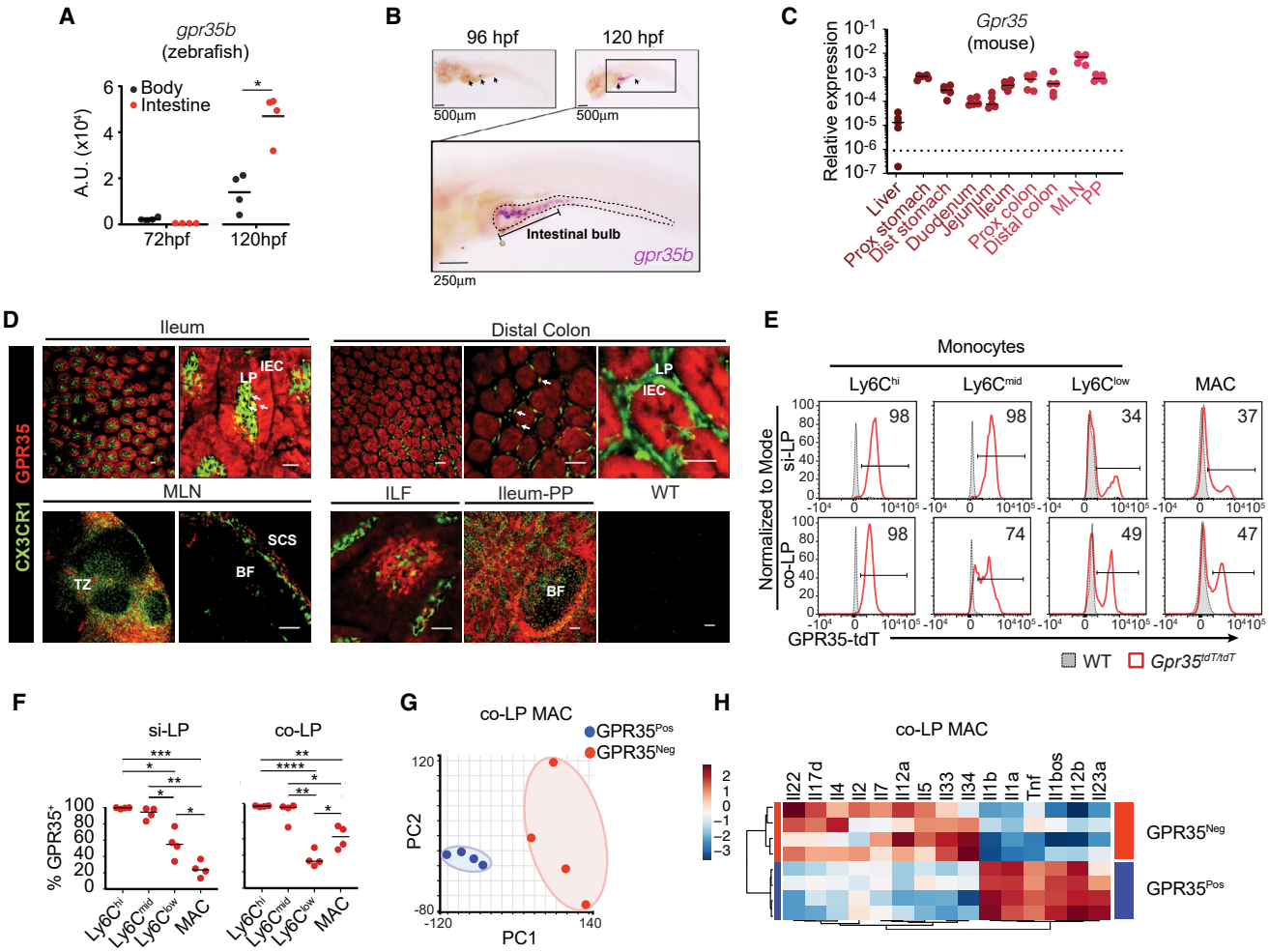

Figure 1. GPR35 Is Expressed in Colonic Macrophages

(A) *gpr35b* mRNA levels by qPCR normalized to *ef1a* across the body and intestines of zebrafish larvae at 72 hpf and 120 hpf. Each dot represents one independent experiment with 20 embryos. A.U., arbitrary units normalized to the lower value (body, 72 hpf).

(B) Whole-mount *in situ* hybridization (WISH) to detect *gpr35b* mRNA expression in zebrafish larvae at 96 hpf and 120 hpf. Arrows indicate the intestinal bulb; dashed lines indicate the intestinal tract. One representative picture is shown from 40 larvae.

(C) *Gpr35* mRNA expression levels by qPCR normalized to *Gapdh* across indicated tissues in WT mice.

(D) *Ex vivo* fluorescence imaging of ileum, distal colon, mesenteric lymph node (MLN), isolated lymph follicle (ILF), and Peyer's patch (PP) from *Cx3cr1*-GFP (green) × *Gpr35*-tdTomato (red) mice. The last panel shows colon from WT as the background control. LP, lamina propria; IEC, intestinal epithelial cell; TZ, T cell zone; BF, B cell follicle; SCS, subcapsular sinus. Arrows indicate CX3CR1^{+} phagocytes that express GPR35. Scale bars, 50 µm.

(E) Representative GPR35-tdTomato expression by flow cytometry in monocyte subsets (Ly6C^{high} to Ly6C^{low}) and macrophages (MACs) from small intestinal and colonic lamina propria (si-LP and co-LP, respectively) of *Gpr35*-tdTomato reporter mice (red open squares) and WT mice (gray squares) as the background control. Numbers in histograms indicate the percentage of GPR35-tdTomato^{+} cells.

(F) Quantification of data from (E) indicating the percentages of GPR35-tdTomato^{+} cells in monocytes and macrophages in the si-LP and co-LP.

(G) Principal-component analysis from RNA-seq of GPR35-tdTomato-positive (GPR35^{pos}) and -negative (GPR35^{neg}) co-LP macrophages.

(H) Heatmap representation of cytokine expression profiles from the RNA-seq in (G).

Data are represented as individual values with medians, with each dot representing one biological replicate. *p < 0.05; **p < 0.01; ***p < 0.001, by two-way ANOVA with Tukey's multiple comparisons test.

See also Figure S1.

Gpr35 Expression Is Microbiota Dependent and Upregulated upon Inflammation

Next, we considered the possibility that the intestinal environment could modulate the expression of GPR35. We found that perturbation of intestinal bacteria by antibiotic treatment resulted in reduced intestinal *gpr35b* transcript levels compared to vehicle-treated zebrafish, as seen with WISH and qPCR (Figures 2A and 2B). Similarly, broad-spectrum antibiotic cocktail administration resulted in decreased *Gpr35* transcripts in the colonic LP compared to non-treated mice (Figure 2C). Unchanged levels in IECs (Figure 2C) suggest that *Gpr35* in the LP, but not the IEC compartment, is responsive to microbiota.

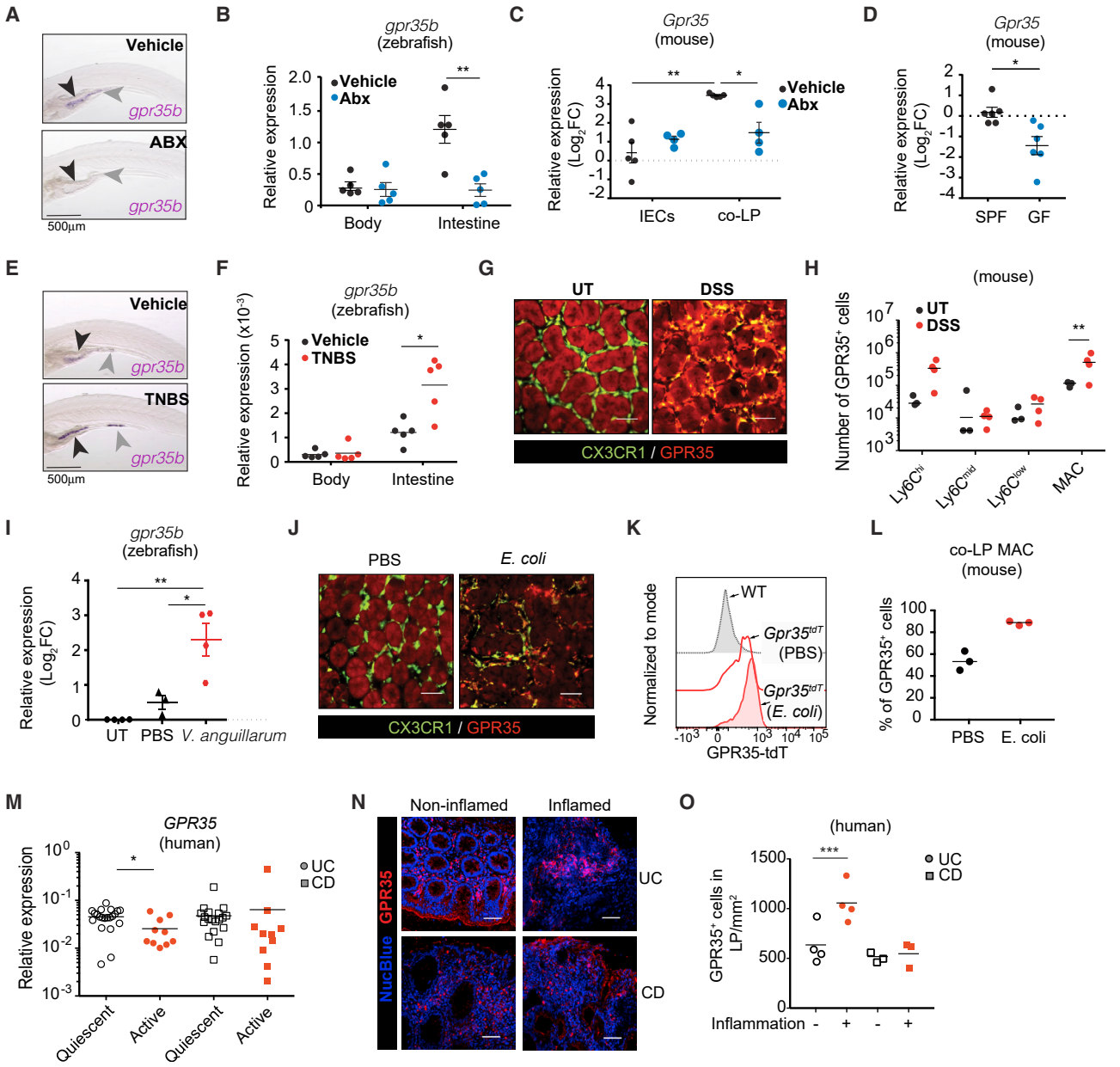

Figure 2. *Gpr35* Expression Is Modulated by the Microbiota and Inflammation

(A) *gpr35b* mRNA expression by WISH in 120-hpf zebrafish larvae treated with antibiotics (ABX) or vehicle. Arrowheads indicate the intestinal bulb. One representative picture is shown from 40 larvae.

(B) *gpr35* mRNA levels by qPCR normalized to *ef1a* in the body and intestines from WT zebrafish treated with antibiotics or vehicle. Each dot represents a pool of 10 larvae (two independent experiments).

(C) *Gpr35* mRNA levels by qPCR normalized to *Hprt* in intestinal epithelial cells (IECs) and colonic lamina propria (co-LP) cells from WT mice treated with an antibiotics cocktail or vehicle daily for 10 days.

(D) *Gpr35* mRNA expression levels by qPCR normalized to *Hprt* in colonic tissue from specific pathogen-free (SPF) and germ-free (GF) mice.

(E) *gpr35b* mRNA expression detected by WISH in 120-hpf zebrafish larvae treated with TNBS or vehicle. Arrowheads indicate intestinal bulb and the posterior intestine. One representative picture is shown from 20 larvae.

(F) *gpr35b* mRNA expression levels by qPCR normalized to *ef1a* in the body and intestines from WT zebrafish treated with TNBS or vehicle. Each dot represents a pool of 10 larvae (two independent experiments).

(G) *Ex vivo* fluorescence imaging of colon from untreated (UT) or DSS-treated *Cx3cr1*-GFP (green) × *Gpr35*-tdTomato (red) mice on day 7 of DSS colitis. Scale bars, 50 µm.

(H) Numbers of GPR35-tdTomato^{+} monocytes (Ly6C^{high} to Ly6C^{low}) and macrophages (MAC) quantified by flow cytometry of co-LP from UT and DSS-treated *Gpr35*-tdTomato mice.

(legend continued on next page)

Analogously, germ-free mice had lower colonic *Gpr35* expression compared to that in specific pathogen-free mice (Figure 2D).

Given that the intestinal epithelium and immune system are in constant exposure to inflammatory stimuli from the luminal content, we hypothesized that *Gpr35* might be modulated by inflammation. Supporting this hypothesis, we found that treating zebrafish with TNBS, which breaks the mucosal barrier (Wirtz et al., 2007) and induces pro-inflammatory cytokines (Figure S2A), resulted in enhanced *gpr35b* transcript levels in the intestinal bulb (Figure 2E, black arrowheads) and ectopic *gpr35b* expression in the posterior intestine (Figure 2E, gray arrowheads). Concomitantly, qPCR revealed higher levels of *gpr35b* transcripts in the intestine of TNBS-treated zebrafish compared to those in vehicle-treated animals (Figure 2F). *Ex vivo* imaging of *Cx3cr1*-GFP × *Gpr35*-tdTomato double-reporter mice revealed increased *Gpr35*-tdTomato signal by CX3CR1$^+$ mononuclear phagocytes in the colons of mice treated with DSS that showed body weight loss and increased disease score (Figures 2G and S2B). Flow-cytometric analysis confirmed an increased number of GPR35$^+$ colonic macrophages in response to DSS (Figure 2H). To determine whether infection-induced inflammation modulates *Gpr35* expression, we injected the swim bladder/intestine region from zebrafish with *Vibrio anguillarum* extracts and quantified *gpr35b* transcripts in the whole larvae. *V. anguillarum*-injected zebrafish showed a ~4-fold increase in *gpr35b* transcripts compared to PBS-treated fish (Figure 2I). In mice not carrying an OVA-specific T cell receptor, we found that colonization of *Cx3cr1*-GFP x *Gpr35*-tdTomato double-reporter mice with *Escherichia coli* DH10B pCFP-OVA (Rossini et al., 2014) induced GPR35 expression in colonic LP macrophages (Figures 2J–2L), providing further evidence that GPR35 expression is modulated in the context of inflammation in a non-antigen-specific manner.

We next sought to test the clinical relevance of GPR35 regulation during colitis. We found decreased *GPR35* expression in UC patients with active disease compared to those with quiescent disease; in contrast, Crohn's disease (CD) patients showed comparable *GPR35* expression between active and quiescent disease in entire tissues (Figure 2M). Since both IECs and macrophages express GPR35, we next performed staining for GPR35 in patient biopsies. We determined the number of GPR35$^+$ cells in the LP of biopsies taken from inflamed or non-inflamed parts of the intestine from the same patients. We found no differences in the numbers of GPR35$^+$ cells between inflamed and non-inflamed regions in CD patients, but we did observe an increase in inflamed regions in patients with UC (Figures 2N and 2O). Taken together, these data indicated that the LP but not the epithelial cells of active UC patients increase their GPR35 expression.

LPA Induces *Tnf* Expression in Macrophages in a GPR35-Dependent Manner

To identify endogenous ligands of GPR35 in the context of intestinal immunity, we focused on LPA, KYNA, and CXL17, which have been previously suggested as GPR35 ligands (Maravillas-Montero et al., 2015; Oka et al., 2010; Wang et al., 2006). We first screened these candidate ligands in a Chinese hamster ovary (CHO)-K1 GPR35 Gi cell line, stably overexpressing human GPR35 naturally coupled to an inhibitory G protein, that inhibits forskolin-induced cyclic AMP (cAMP) accumulation in response to GPR35 agonists. As expected, stimulation with the synthetic GPR35 agonist zaprinast (Mackenzie et al., 2011) inhibited forskolin-induced cAMP production (Figure 3A). KYNA did not elicit a significant response, whereas LPA and CXCL17 inhibited cAMP production, with LPA exerting its effect at a lower concentration compared to CXCL17 (Figure 3A). To investigate the outcome of LPA-mediated GPR35 activation *in vivo*, we took advantage of CRISPR-Cas9-based genome engineering of zebrafish (Li et al., 2016) to generate a *gpr35b* mutant line (*gpr35b*^{uu1892}) (Figures S3A and S3B) that was viable and fertile and did not exhibit any noticeable defect in development while in homozygosis (data not shown). 48 h of either Zap or LPA treatment resulted in elevated expression of pro-inflammatory cytokines, including *tnf*, *il1b*, and *il17a/f* in wild-type (WT) zebrafish larvae; however, none of these cytokines were induced by either Zap or LPA in the *gpr35b*^{uu19b2} mutants (Figure 3B), indicating *gpr35b* dependency. Of note, a visible tendency is observed in untreated larvae, in which the level of cytokines seems to be lower in *gpr35b*^{uu1892} mutants compared to WT larvae (Figure 3B), suggesting that endogenous LPA might be produced at early developmental stages. To translate our findings in mice, we used CRISPR-Cas9 to generate a *Gpr35* knockout (KO) mouse line (Figure S3C). The resulting *Gpr35*-KO mice failed to show GPR35 staining by immunofluorescence (Figure S3D) and showed comparable numbers of dendritic cells, neutrophils, monocytes, and macrophages in the colonic LP (Figure S3E), indicating that lack of GPR35 did not alter the colonic myeloid compartment. To investigate whether GPR35 is required for myeloid cell function, we analyzed the transcriptomic profile of WT and GPR35-deficient BMDMs upon lipopolysaccharide (LPS) or LPA stimulation. Comparable transcriptomic

(I) *gpr35b* mRNA expression levels measured by qPCR normalized to *ef1a* in WT zebrafish exposed to PBS or *V. anguillarum*. Each dot represents a pool of 10 larvae (two independent experiments).
(J) *Ex vivo* fluorescence imaging of colons from *Cx3cr1*-GFP (green) × *Gpr35*-tdTomato (red) mice gavaged with PBS or *E. coli* on day 21. Scale bars, 50 μm.
(K) Representative *Gpr35*-tdTomato expression by flow cytometry in co-LP macrophages from WT (gray histogram), PBS-gavaged (red open histogram), and *E. coli*-gavaged *Cx3cr1*-GFP x *Gpr35*-tdTomato (red filled histogram) mice.
(L) Quantification of flow-cytometric data from (K) for numbers of GPR35$^+$ cells in co-LP macrophages.
(M) *GPR35* mRNA expression by qPCR in biopsies from ulcerative colitis (UC) or Crohn's disease (CD) patients with quiescent or active disease.
(N) Immunofluorescence imaging of UC or CD patient biopsies from non-inflamed (left) or inflamed regions (right). Sections were stained for GPR35 (red) and NucBlue (blue) for nuclear staining. Scale bars, 50 μm.
(O) Number of GPR35$^+$ cells in the lamina propria per square millimeter quantified by manual counting of immunofluorescence images shown in (N).
Data are represented as individual values, with medians with each dot representing one biological replicate. *p < 0.05; **p < 0.01; ***p < 0.001, by unpaired t test in (D); one-way ANOVA in (I) or two-way ANOVA with Tukey's multiple comparisons test in (B), (C), (F), (H), and (O); or Mann-Whitney in (L) and (M).
See also Figure S2.

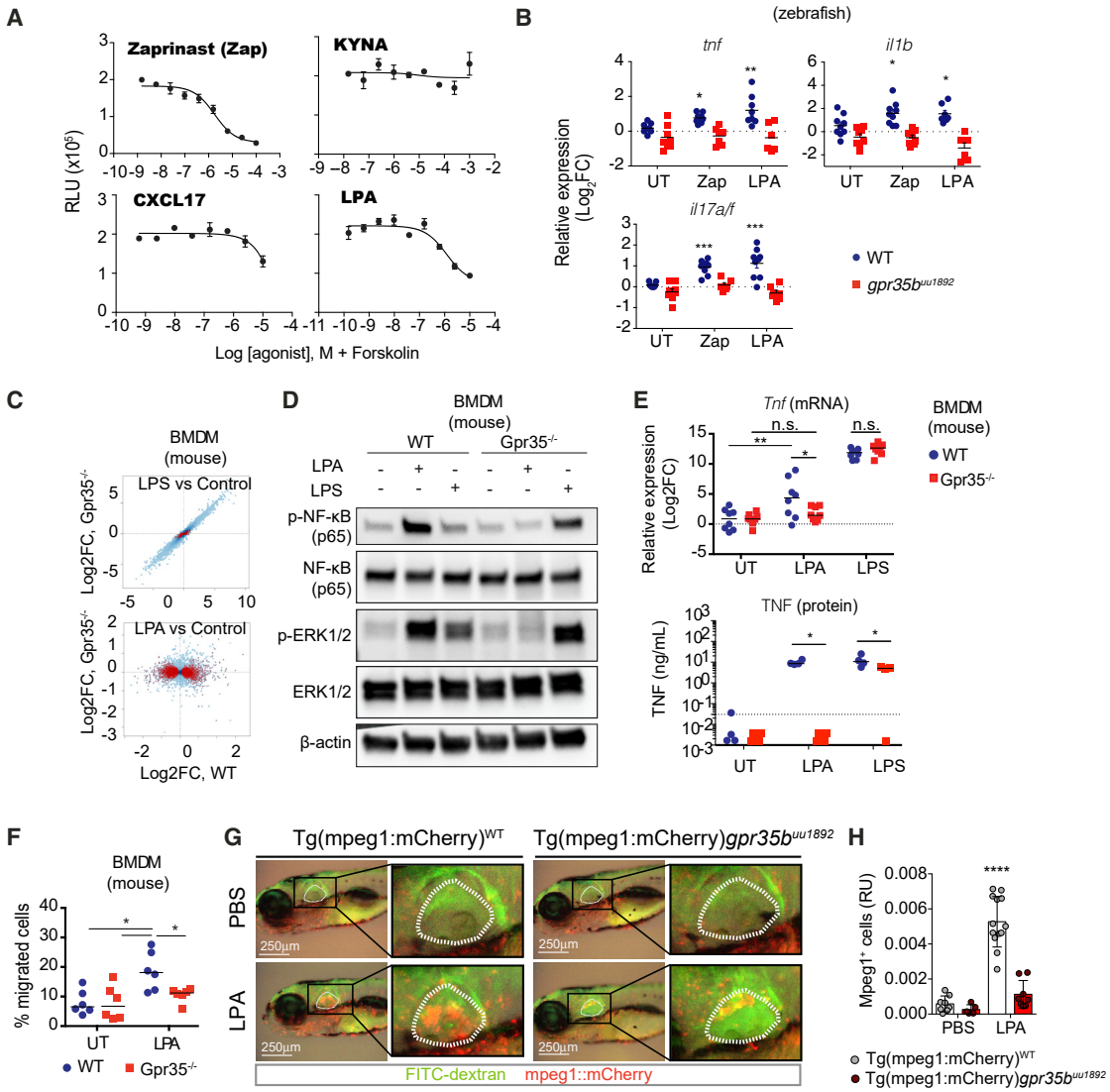

Figure 3. LPA Induces *Tnf* Expression in a GPR35-Dependent Manner

(A) Relative luminescence unit (RLU) values for intracellular cAMP levels in Gi-coupled GPR35-transfected CHO-K1 cells in response to forskolin against serial dilutions of zaprinast, KYNA, CXCL17, or LPA. Data are represented as median plus or minus the range from doublets with nonlinear fit curves.

(B) mRNA expression levels of *tnf*, *il1b*, and *il17a/f* measured by qPCR in untreated (UT) or LPA-treated WT or *gpr35b*^{uu1892} zebrafish larvae. Each dot represents a pool of 10 larvae (three independent experiments).

(C) Fold changes in mRNA expression from the RNA-seq of control and LPA- or LPS-treated BMDMs from WT or *Gpr35*$^{-/-}$ mice. Each dot represents a gene, and red dots indicate genes that are significantly regulated in WT cells in response to stimuli compared to control.

(D) Western blot analysis of cell lysates of control, LPA-treated, and LPS-treated BMDMs from WT or *Gpr35*$^{-/-}$ mice for phosphorylated and total NF-κB (p65) and ERK1/2. β-actin was used as protein loading control.

(E) mRNA expression levels of *Tnf* by qPCR in UT or LPA-treated BMDMs from WT or *Gpr35*$^{-/-}$ mice (upper panel). Results are cumulative of three independent experiments. Concentrations of TNF in supernatants of BMDMs by the LEGENDplex bead-based immunoassay (lower panel).

(F) Percentages of migrated BMDMs from WT or *Gpr35*$^{-/-}$ mice toward UT control or LPA in Transwell assay by flow cytometry. Results are cumulative of three independent experiments in which each dot represents one mouse.

(G) Macrophage recruitment (mpeg1+ cells) in *Tg(mpeg1:mCherry)*^{WT} and *Tg(mpeg1:mCherry)gpr35b*^{uu1892} zebrafish larvae injected with DMSO or LPA in the otic vesicle (white dashed line). Results are cumulative of two independent experiments in which every dot represents one embryo.

(H) Quantification of macrophage recruitment data as shown in (E) for numbers of mpeg1^{+} cells in otic vesicles.

Data are represented as individual values with medians. *p < 0.05; **p < 0.01; ***p < 0.001, by two-way ANOVA with Tukey's multiple comparisons test. n.s., not significant.

See also Figures S3 and S4.

profiles were observed in LPS-treated WT and GPR35-deficient BMDMs (Figure 3C, upper plot), indicating that GPR35-deficient BMDMs are not impaired in sensing LPS. By contrast, the transcriptome profiles were dramatically different between WT and GPR35-deficient BMDMs upon stimulation with LPA (Figure 3C, lower plot), indicating that LPA induces a specific transcriptomic profile that depends on GPR35. In order to gain mechanistic insights into the signaling pathways downstream of LPA-mediated GPR35 activation, we analyzed the activation of ERK and nuclear factor κB (NF-κB). Both ERK and NF-κB (p65) phosphorylation were reduced in GPR35-deficient compared to WT BMDMs upon exposure to LPA but not LPS (Figures 3D and S4B–S4D). By contrast, LPS, but not LPA, induced substantial STAT3 phosphorylation in WT and GPR35-deficient BMDMs (Figures S4A and S4E), further confirming that LPA triggers specific pathways in macrophages in a GPR35-dependent manner. Having demonstrated that LPA signals through GPR35 in murine macrophages, we next sought to validate the cytokine profile observed in zebrafish upon LPA stimulation. In line with the zebrafish data, stimulation of WT murine BMDMs with LPA significantly induced *Tnf* mRNA levels, which was absent in *Gpr35*$^{-/-}$ BMDMs (Figure 3E), whereas LPS did not result in differential regulation of *Tnf*. Modulation of TNF at the protein level was confirmed by bead-based immunoassay, as seen by reduced TNF concentrations in LPA-stimulated G*pr35*$^{-/-}$ compared to WT BMDMs (Figure 3E). TNF production in response to LPS in *Gpr35*$^{-/-}$ BMDMs was also decreased but to a lower extent in comparison to LPA. On the other hand, the modulation of interleukin (IL)-1β and IL-23 transcript and protein levels on LPA stimulation was not reproduced in murine macrophages (Figures S4F and S4G). Altogether, our data indicate that LPA-mediated GPR35 signaling in macrophages results in a distinct transcriptional profile, characterized by TNF production, which was associated with ERK and NF-κB activation.

Given that LPA increases the migration of monocytes, microglia, and ovarian cancer cells (Oh et al., 2017; Plastira et al., 2017; Takeda et al., 2019), we next tested whether LPA acts as a chemoattractant for macrophages. We quantified the migration of WT and *Gpr35* KO BMDMs in response to LPA in a transwell migration system, which revealed that *Gpr35*-deficient BMDMs had reduced migration in response to LPA compared to WT BMDMs (Figure 3F). To investigate the LPA-GPR35 axis in modulating macrophage chemotaxis *in vivo*, we crossed *gpr35b*^{uu1892} mutant zebrafish with the reporter strain *Tg(mpeg1:mCherry)* to visualize macrophage dynamics as previously described (Nguyen-Chi et al., 2015). Injection of LPA within the otic vesicle resulted in increased macrophage infiltration compared to PBS injection in WT reporter fish. By contrast, macrophages in *gpr35b*^{uu1892} mutant fish did not respond to LPA injection (Figures 3G and 3H), indicating that LPA induces chemotaxis of macrophages *in vivo* in a GPR35-dependent fashion.

Intestinal Inflammation Increases Autotaxin Expression in Zebrafish and Mice

LPA is a phospholipid derivate found in cell membranes and cell walls that can act as an extracellular signaling molecule (Ye and Chun, 2010). LPA is mainly synthesized by autotaxin (ATX), which removes a choline group from lysophosphatidylcholine (Gesta et al., 2002). Therefore, we investigated whether ATX is induced during intestinal inflammation *in vivo*, which revealed a 2-fold increase in *atx* transcripts in intestinal tissues isolated from TNBS-treated compared to untreated zebrafish larvae (Figure 4A). Pursuing these findings in mice, we first consulted our published longitudinal transcriptomic data from mice undergoing DSS colitis (Czarnewski et al., 2019), which showed transient colonic *Tnf*, *Ifn*, *Il17a*, and *Il6* expression (Figure 4B), and we found that *Atx* expression peaked at day 10 (Figure 4C), which is behind the peak of *Tnf*, *Ifn*, *Il17a*, and *Il6* expression. Consistently, mice with DSS-induced intestinal inflammation showed an increased number of ATX^{+} cells in colonic tissues as inflammation progressed (Figures 4D and 4E). Notably, *Gpr35*$^{-/-}$ mice exposed to DSS showed a comparable increase in the number of ATX^{+} cells compared to WT mice exposed to DSS (Figure 4F). To determine whether upregulated ATX correlates with LPA synthesis, we took the supernatants of colonic explants from DSS-treated WT and *Gpr35*$^{-/-}$ mice and measured LPA levels by ELISA (Figure 4G). DSS-treated mice showed increased LPA levels independent of GPR35. In conclusion, colitis in zebrafish and mice led to increased *Atx* expression, which was associated with increased LPA production within the colon.

Macrophage-Specific Deletion of *Gpr35* Exacerbates DSS Colitis

Given that GPR35 activation modulated cytokine production and macrophage migration together with the potential LPA synthesis during DSS-induced colitis, we hypothesized that GPR35 might affect intestinal inflammation. We exposed WT and G*pr35*$^{-/-}$ mice to DSS and evaluated the degree of colitis. *Gpr35*-deficient mice had exacerbated colitis compared to WT animals, as indicated by elevated body weight loss, increased disease activity scores, shorter colons, and higher histological colitis scores (Figures S5A–S5F). We next sought to define the cell type(s) underlying the worsened colitis in *Gpr35*-deficient mice. Since GPR35 is expressed by both IECs and CX3CR1^{+} macrophages, we generated *Gpr35*^{flox} mice by adding loxP sites before exon 2 and after 3′ UTR regions of *Gpr35* (Figure S5G) and crossed *Gpr35*^{flox} with *Cx3cr1*^{CreER} mice to obtain tamoxifen-inducible *Gpr35*$^{\Delta Cx3cr1}$ mice. This cross yielded mice with tamoxifen-inducible deletion of *Gpr35* specifically in CX3CR1^{+} macrophages confirmed by immunofluorescent staining for GPR35 (Figures S5H and S5I) and not resulting in substantial changes of colonic monocyte and macrophage numbers (Figures S5J and S5K). *Gpr35*$^{\Delta Cx3cr1}$ mice displayed aggravated colitis compared to other control groups, as demonstrated by significant body weight loss, increased disease activity scores, reduced colon length, and increased endoscopic and histological colitis scores (Figures 5A–5F and S5L). We then treated WT and *Gpr35*$^{\Delta Cx3cr1}$ daily with 5 mg/kg LPA, a concentration that protects against endotoxin-induced acute kidney injury (Mirzoyan et al., 2017). LPA treatment resulted in reduced body weight loss, disease activity scores, and endoscopic and histological colitis scores in WT but not in *Gpr35*$^{\Delta Cx3cr1}$ mice (Figures 5G–5L, S5M, and S5N).

Consistent with enhanced inflammation, flow-cytometric analysis revealed increased percentages and numbers of neutrophils

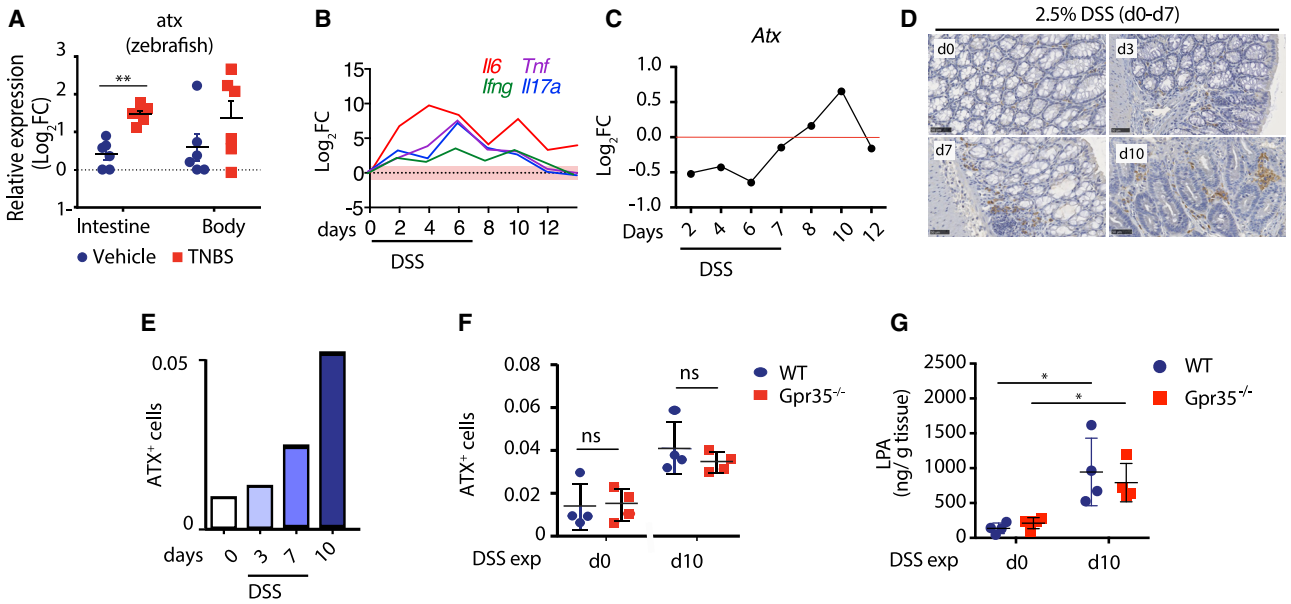

Figure 4. Colitis Induces Expression of the LPA-Generating Enzyme ATX

(A) *Autotaxin* (*atx*) mRNA levels by qPCR normalized to *ef1a* in the body and intestine of WT zebrafish treated with TNBS or vehicle. Each dot represents a pool of 10 larvae (two independent experiments).

(B and C) RNA-seq analysis showing (B) *Il17a*, *Il6*, *Tnf*, and *Ifng* and (C) *Atx* gene expression from colon during 2.5% DSS-induced colitis (7-day exposure) and recovery. Dots indicate the average from three different mice per data point.

(D) Immunohistochemistry imaging of WT mice treated with 2.5% DSS at indicated time points; brown indicates ATX, and blue indicates H&E. One representative experiment is indicated from two experiments. Scale bars, 50 μm. d, day.

(E) Quantification of ATX$^+$ cell data from (C). One representative experiment is indicated from two experiments.

(F) Quantification of ATX$^+$ cells from colonic tissue at day 0 and day 10 of WT and *Gpr35*$^{-/-}$ mice treated with DSS. ns, not significant.

(G) LPA concentrations in colonic explant supernatants of WT and *Gpr35*$^{-/-}$ mice on days 0 and 7 by ELISA.

Data are represented as individual values with mean ± SD. *p < 0.05; **p < 0.01; ***p < 0.001, by two-way ANOVA with Tukey's multiple comparisons test.

in *Gpr35*$^{\Delta Cx3cr1}$ compared to control mice, further indicating exacerbated inflammation (Figures S6A–S6C), which was not accompanied with higher macrophage infiltration into the colonic LP of *Gpr35*$^{\Delta Cx3cr1}$ mice (Figures S6A–S6C).

TNF Attenuates Exacerbated DSS Colitis in *Gpr35*$^{\Delta Cx3cr1}$ Mice

Gpr35$^{\Delta Cx3cr1}$ mice with DSS colitis showed reduced frequencies and mean fluorescence intensity of TNF-producing macrophages (Figures 6A and 6B), although significant changes in overall expression of *Tnf*, *Il10*, *Il1b*, or *Il6* in colonic tissue was not observed (Figure S6D).

Despite the well-known pro-inflammatory properties of TNF and its pathogenic role in human IBD, some studies have suggested anti-inflammatory properties for TNF in the context of DSS colitis, where TNF neutralization or *Tnf* deficiency exacerbates symptoms (Naito et al., 2003; Noti et al., 2010). We, therefore, investigated whether exacerbated colitis in *Gpr35*$^{\Delta Cx3cr1}$ mice was due to the inability of CX3CR1$^+$ macrophages to produce TNF. To address this hypothesis, we injected *Gpr35*$^{\Delta Cx3cr1}$ mice daily with 1 μg TNF, a concentration previously shown to restore corticosterone synthesis in colitis models (Noti et al., 2010). This treatment resulted in reduced colitis severity compared to untreated *Gpr35*$^{\Delta Cx3cr1}$ mice, as indicated by decreased body weight loss, reduced disease activity scores, longer colon length, reduced endoscopic signs of colitis, and histologic colitis scores (Figures 6C–6H). Given that TNF can induce the expression of *Cyp11a1* and *Cyp11b1*, which encode steroidogenic enzymes involved in the synthesis of corticosterone in IECs and thereby can attenuate the severity of DSS colitis (Noti et al., 2010), we measured *Cyp11a1* and *Cyp11b1* expression in the colons of these mice. Expression of *Cyp11b1*, but not *Cyp11a1*, was reduced in *Gpr35*$^{\Delta Cx3cr1}$ mice (Figures 6I and 6J), and injection of TNF in *Gpr35*$^{\Delta Cx3cr1}$ mice restored *Cyp11b1* expression during colitis (Figure 6J). By contrast, TNF treatment of WT animals did not affect colitis severity or *Cyp11b1* and *Cyp11a1* expression (Figures S7A–S7I). These data suggest that the administered TNF does not affect colitis in WT mice as opposed to its protective effect in *Gpr35*$^{\Delta Cx3cr1}$ animals. Consistent with these findings, supernatants of colonic explants from *Gpr35*$^{\Delta Cx3cr1}$ mice had lower corticosterone concentrations compared to WT animals with colitis. TNF injection resulted in significantly increased corticosterone concentrations in supernatants of colonic explants compared to explants from untreated *Gpr35*$^{\Delta Cx3cr1}$ mice with colitis (Figure 6K). Taken together, these results demonstrate that loss of *Gpr35* in macrophages leads to aggravated colitis that is associated with reduced *Cyp11b1* expression in the intestine; notably, TNF injection correlated with reversed *Cyp11b1* expression and colitis severity in *Gpr35*$^{\Delta Cx3cr1}$ mice.

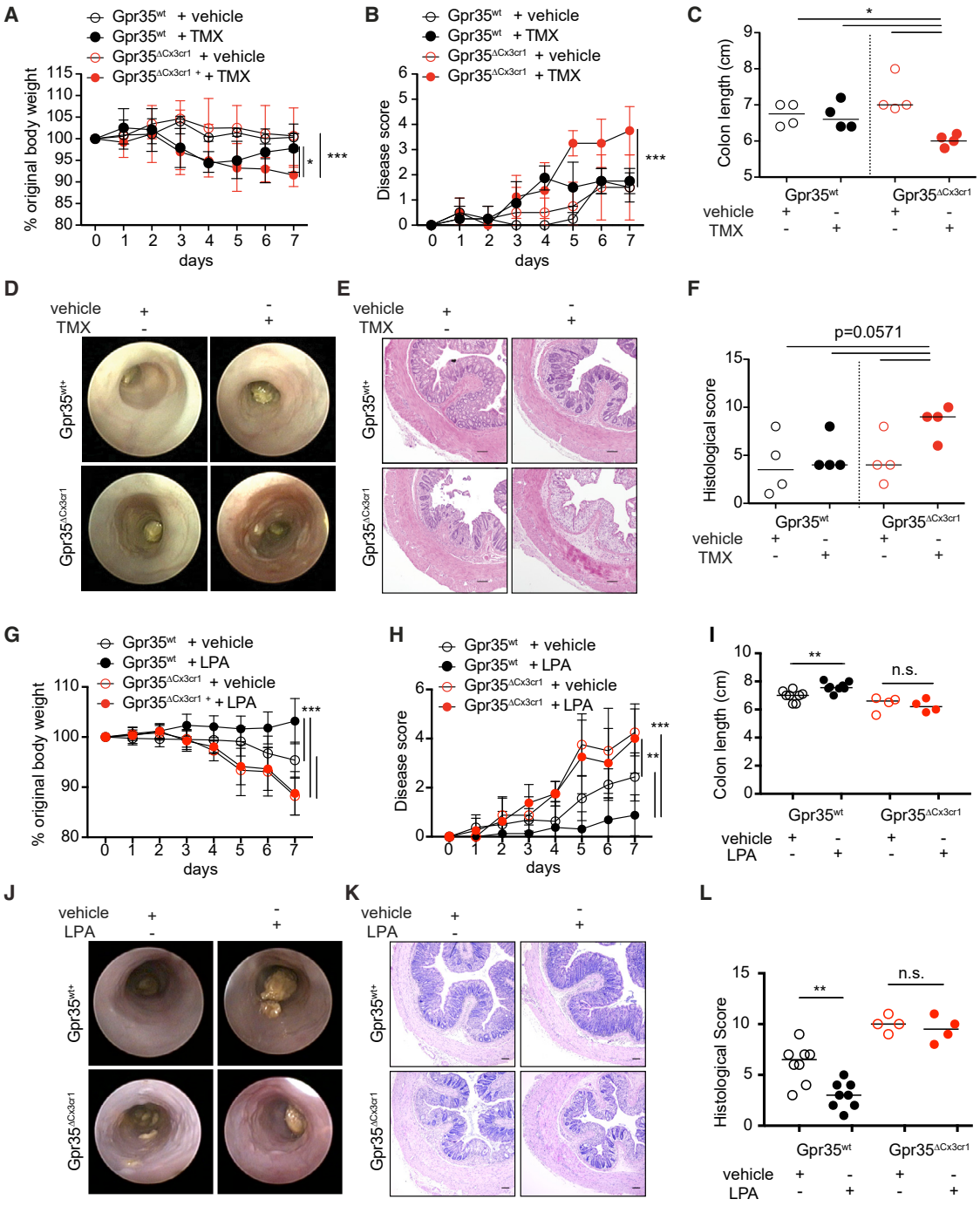

Figure 5. Deletion of *Gpr35* in CX3CR1^{+} Macrophages Exacerbates DSS-Induced Colitis

(A) Body weight changes (normalized to initial weight).

(B) Disease activity scores during DSS colitis for 7 days of vehicle-injected (corn oil) or tamoxifen (TMX)-injected *Gpr35^{wt}* or *Gpr35$^{\Delta Cx3cr1}$* mice. Data are indicated as mean ± SD for four mice per group.

(C) Colon lengths on day 7 complementary to data in Figure S5L.

(D and E) Endoscopic images (D) and representative H&E images (E) of colons from vehicle- or TMX-treated *Gpr35^{wt}* or *Gpr35$^{\Delta Cx3cr1}$* mice with DSS colitis. Scale bars, 100 μm.

(F) Histology scores quantified from (E).

(G) Body weight changes shown as percentage of initial body weights.

(legend continued on next page)

The Hyperactive GPR35^{T108M} Variant Is Associated with Treatment Success of TNF Blockers

To gain insights into the function of the human variant of GPR35, we took advantage of the CD and UC patients enrolled in the Swiss IBD Cohort Study carrying the GPR35 coding variant rs3749171, in which C is replaced by T leading to a hyperactive T108M missense variant (Schneditz et al., 2019). We investigated whether these patients were associated with either breakthrough/loss of response, primary non-response (never effective), and/or side effects/intolerance in response to TNF blockers. We observed that the hyperactive GPR35^{T108M} variant resulted in an increased percentage of treatment success in response to TNF blockers (Table 1), suggesting that the GPR35^{T108M} variant might be an indication of anti-TNF therapy responsiveness in IBD patients.

DISCUSSION

It has been proposed that the recognition of host- and/or microbial-derived metabolites by G-protein-coupled receptors (GPCRs) plays a critical role in driving cytokine responses in the context of infection or IBD (Chen et al., 2019; Cohen et al., 2017). In this study, we used a combination of genetic mouse and zebrafish models to study the biological relevance of GPR35 signaling, the dysfunction of which has been associated with increased IBD susceptibility.

Previous studies have suggested several potential ligands of GPR35; however, depending on the experimental settings and/or species, the results have been inconsistent (Binti Mohd Amir et al., 2018; Mackenzie et al., 2011; Maravillas-Montero et al., 2015; Oka et al., 2010; Southern et al., 2013). Because interspecies variation in ligand pharmacology must be considered for GPR35 (Milligan, 2018), we used genetic zebrafish and mouse models that lack GPR35. Using this comparative approach, we showed remarkably conserved inflammatory cytokine production upon LPA stimulation, which was GPR35 dependent. Moreover, mouse and zebrafish macrophages responded to LPA as a chemoattractant in a GPR35-dependent manner. Although we demonstrated that GPR35 was required in bone-marrow-derived macrophages *in vitro*, our *in vivo* zebrafish experiments did not allow us to rule out that other GPR35^{+}-expressing cells sense LPA to then induce macrophage recruitment. Whether GPR35-dependent chemotaxis contributes to intestinal homeostasis and disease remains to be investigated. However, our findings suggest that LPA can activate GPR35 in zebrafish and mice, demonstrating that LPA-induced GPR35 signaling is conserved across species.

We found that both mice and zebrafish showed increased expression of *Atx*, which catalyzes the LPA formation (Gesta et al., 2002), during inflammation. Importantly, *Atx* expression was associated with LPA production, suggesting that LPA might regulate the extent of intestinal inflammation. However, the degree to which host cells and/or microbiota contribute to LPA production has not been fully explored. One possibility is that the disruption of epithelial cells leads to the release of LPA or precursors that are further metabolized by LP cells expressing ATX. Phospholipids derived from microorganisms that constitute the intestinal microbiota may be another source of LPA during colitis (Cullinane et al., 2005). One recent study used mass spectrometry to distinguish microbial-derived versus host-derived metabolites by stable isotope tracing of ^{13}C-labeled live non-replicating *E. coli* from ^{12}C host isotypes (Uchimura et al., 2018). Our analysis of these published mass spectrometry data indicated that both host cells and microbes contribute to the LPA content in the colon. Importantly, our data, in which administration of LPA ameliorates intestinal inflammation in WT but not GPR35-deficient animals, suggest that the LPA-GPR35 axis is important for the re-establishment of intestinal homeostasis upon inflammation. However, whether LPA plays a role and the potential source during intestinal inflammation in IBD patients carrying the *GPR35* variant remain to be explored.

TNF is a well-described pro-inflammatory cytokine central to the pathogenesis of Crohn's disease and UC (Reinecker et al., 1993). As a consequence, the inhibition of TNF with antibodies ameliorates colitis in animal models, and anti-TNF antibodies are essential for the treatment of patients with IBD (Corazza et al., 1999; Neurath et al., 1997; Present et al., 1999; Sands et al., 2001; Siegel et al., 1995). Our data suggest a model in which GPR35 signaling in macrophages induces TNF expression, which is beneficial to maintain intestinal homeostasis, and this might contradict the paradigm that TNF is pathogenic in IBD. In this line, some studies have shown that TNF has anti-inflammatory effects in the context of *Tnf*-deficient animals, which result in more severe DSS colitis (Naito et al., 2003; Noti et al., 2010). TNF is quickly released after tissue damage to reduce damage-associated mortality (Mizoguchi et al., 2008). Our data show that GPR35-dependent TNF induction results in the induction of corticosterone production, which might suppress immune responses. Therefore, TNF can play a protective or deleterious role depending on the context and stage of the disease. On the other hand, studies in macrophages carrying the IBD-associated T108M polymorphism in GPR35 result in enhanced metabolic activity compared to the wild-type GPR35, which is the opposite effect compared to GPR35 loss of function (Schneditz et al., 2019; Tsukahara et al., 2017). These data suggest the

(H) Disease activity scores for DSS colitis parameters assessed daily for 7 days of vehicle- or LPA-injected *Gpr35^{wt}* or *Gpr35$^{\Delta Cx3cr1}$* mice. Data are indicated as mean ± SD for four mice per group.

(I) Colon lengths measured from Figure S5M.

(J and K) Representative endoscopy images (J) and H&E staining (K) of colons corresponding to day 7 of DSS colitis from *Gpr35^{wt}* or *Gpr35$^{\Delta Cx3cr1}$* mice that received daily vehicle or LPA injections.

(L) Histological DSS colitis scores calculated from (K).

Each dot represents one animal with medians, unless stated otherwise. *$p < 0.05$; **$p < 0.01$; ***$p < 0.001$, by two-way ANOVA with Tukey's multiple comparisons test in (A), (B), (G), and (H) or Mann-Whitney in (C), (F), (I), and (L). n.s., not significant.

See also Figures S5 and S6.

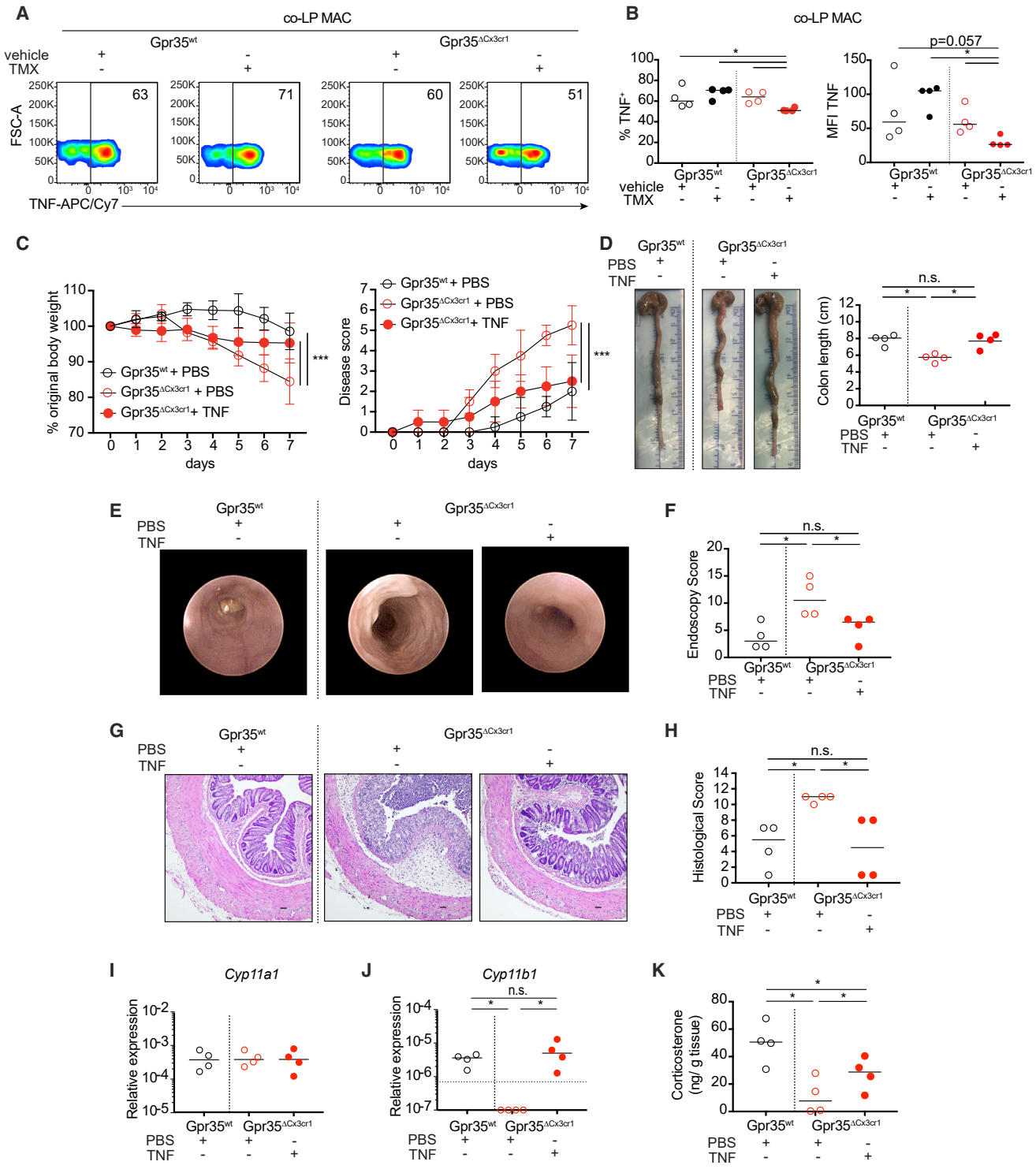

Figure 6. TNF Treatment of *Gpr35*$^{\Delta Cx3cr1}$ Mice Attenuates Colitis

(A) TNF-producing co-LP MAC from vehicle- or TMX-treated *Gpr35*^{wt} or *Gpr35*$^{\Delta Cx3cr1}$ mice by flow cytometry on day 7 of DSS colitis. Numbers in density plots indicate the percentage of TNF^{+} cells.

(B) Percentages and mean fluorescence intensity (MFI) of TNF^{+} cells in macrophages based on flow cytometry data in (A).

(C) Body weight changes (normalized to initial weight) and disease activity scores during 7 days of DSS exposure from PBS-injected *Gpr35*^{wt} (WT) and PBS- or TNF-injected tamoxifen-treated *Gpr35*$^{\Delta Cx3cr1}$ mice. Data are indicated as mean ± SD for four mice per group.

(legend continued on next page)

Table 1. Anti-TNF Blocker Responses among IBD Patients with GPR35^{T108M} Variant

	n (%) for Ulcerative Colitis			n (%) for Crohn's Disease			n (%) for All		
	Success	Failure	Total	Success	Failure	Total	Success	Failure	Total
C	2 (22.22)	7 (77.78)	9 (100)	13 (36.11)	23 (63.89)	36 (100)	15 (33.33)	30 (66.67)	45 (100)
CT	0	0	0	0	3 (100)	3 (100)	0	3 (100)	3 (100)
T	7 (36.84)	12 (63.16)	19 (100)	25 (42.37)	34 (57.63)	59 (100)	33 (41.77)	46 (58.23)	79 (100)
Total	9 (32.14)	19 (67.86)	28 (100)	38 (38.77)	60 (61.23)	98 (100)	48 (37.80)	79 (62.20)	127 (100)

For ulcerative colitis, Pearson $\chi^2(2) = 0.5985$; Probability (Pr) = 0.439. For Crohn's disease, Pearson $\chi^2(2) = 0.3653$; Pr = 0.546. For all, Pearson $\chi^2(2) = 0.8605$; Pr = 0.3536. C, cytosine; T, thymine.

possibility that IBD patients carrying the T108M polymorphism might have enhanced TNF production, resulting in aberrant inflammatory immune responses. This hyperactive T108M polymorphism resulted in an increased treatment success to TNF blockers in the Swiss IBD Cohort Study.

We cannot exclude the possibility that other endogenous ligands may bind to GPR35 and that LPA may also modulate intestinal homeostasis by binding to other LPA receptors. Before GPR35 can be considered as a possible target in the clinic for the treatment of IBD, better pharmacological screenings must be considered to identify additional putative ligands and interspecies variations of potential ligands. Identifying possible connections between host- and microbial-derived metabolites with the immune system will be critical in dissecting mucosal immune responses in healthy individuals and during colitis.

STAR★METHODS

Detailed methods are provided in the online version of this paper and include the following:

- KEY RESOURCES TABLE
- RESOURCE AVAILABILITY
  - Lead Contact
  - Materials Availability
  - Data and Code Availability
- EXPERIMENTAL MODEL AND SUBJECT DETAILS
  - Mouse lines
  - Generation of Gpr35-IRES-tdTomato knock-in mice
  - Generation of Gpr35-flox and knock-out (KO) mice
  - Zebrafish lines
  - Primers used for fluorescence PCR
  - Human inflammatory bowel disease biopsies
- METHOD DETAILS
  - Dextran sodium sulfate induced colitis mouse model
  - Hematoxylin-eosin (H&E) staining and histological scoring
  - Mouse Endoscopy
  - Treatment of zebrafish with 2,4,6-Trinitrobenzenesulfonic acid or with antibiotics
  - Treatment of mice with antibiotics
  - Preparation of sense and antisense Digoxigenin (DIG)-labeled RNA probes for detection of Gpr35b in zebrafish
  - *In situ* hybridization for gpr35b detection in zebrafish
  - Challenging of mice with *E. coli*-CFP
  - Exposure of zebrafish with Vibrio anguillarum
  - LPA injection in zebrafish
  - Stimulation of zebrafish larvae with LPA
  - Cell Isolation from the small and large intestinal lamina propria, mesenteric lymph nodes and spleen
  - Antibodies, cell staining and flow cytometry
  - RNA extraction and quantitative PCR
  - Immunofluorescence staining
  - Autotaxin staining
  - *Ex vivo* imaging of colonic tissues
  - RNA sequencing
  - 3′-5′-Cyclic adenosine monophosphate (cAMP) assay
  - Mouse bone marrow-derived macrophages
  - Cytokine detection by LEGENDplex™ bead-based immunoassay
  - Western blot analysis of LPA- or LPS- treated BMDMs
  - Transwell migration assay for quantification of BMDM migration
  - Enzyme-linked immunosorbent assays (ELISA) for corticosterone and LPA detection

(D) Colon lengths for *Gpr35^{wt}* and PBS- or TNF-injected tamoxifen-treated *Gpr35$^{\Delta Cx3cr1}$* mice.
(E) Endoscopic images of *Gpr35^{wt}* and PBS- or TNF-injected tamoxifen-treated *Gpr35$^{\Delta Cx3cr1}$* mice.
(F) Quantified endoscopic scores from (E).
(G) Representative H&E images of colon of PBS-injected *Gpr35^{wt}* and PBS- or TNF-injected tamoxifen-treated *Gpr35$^{\Delta Cx3cr1}$* mice on day 7 of DSS colitis. Scale bar, 50 μm.
(H) Histology scores for *Gpr35^{wt}* and PBS- or TNF-injected tamoxifen-treated *Gpr35$^{\Delta Cx3cr1}$* mice.
(I and J) mRNA expression levels of *Cyp11a1* (I) and *Cyp11b1* (J) relative to *Actb* by qPCR in colon.
(K) Corticosterone concentration in supernatants of colonic explants of PBS-injected *Gpr35^{wt}* and PBS- or TNF-injected tamoxifen-treated *Gpr35$^{\Delta Cx3cr1}$* mice on day 7 of DSS colitis. Concentrations are normalized to weights of colonic tissues.
Data are presented as individual values with medians. Each dot represents one biological replicate. *p < 0.05; **p < 0.01; ***p < 0.001, by two-way ANOVA with Tukey's multiple comparisons test in (C) and (D) or Mann-Whitney in (B), (F), and (H)–(K). n.s., not significant.
See also Figures S6 and S7.

SUPPLEMENTAL INFORMATION

Supplemental Information can be found online at https://doi.org/10.1016/j.celrep.2020.107979.

CONSORTIA

The members of Swiss IBD Cohort Investigators are: Karim Abdelrahman, Gentiana Ademi, Patrick Aepli, Claudia Anderegg, Anca-Teodora Antonino, Eva Archanioti, Eviano Arrigoni, Diana Bakker de Jong, Bruno Balsiger, Polat Bastürk, Peter Bauerfeind, Andrea Becocci, Dominique Belli, José M. Bengoa, Luc Biedermann, Janek Binek, Mirjam Blattmann, Stephan Boehm, Tujana Boldanova, Jan Borovicka, Christian P. Braegger, Stephan Brand, Lukas Brügger, Simon Brunner, Patrick Bühr, Sabine Burk, Bernard Burnand, Emanuel Burri, Sophie Buyse, Dahlia-Thao Cao, Ove Carstens, Dominique H. Criblez, Sophie Cunningham, Fabrizia D'Angelo, Philippe de Saussure, Lukas Degen, Joakim Delarive, Christopher Doerig, Barbara Dora, Susan Drerup, Mara Egger, Ali El-Wafa, Matthias Engelmann, Jessica Ezri, Christian Felley, Markus Fliegner, Nicolas Fournier, Montserrat Fraga, Remus Frei, Pascal Frei, Michael Fried, Florian Froehlich, Raoul Ivano Furlano, Luca Garzoni, Martin Geyer, Laurent Girard, Marc Girardin, Delphine Golay, Ignaz Good, Ulrike Graf Bigler, Beat Gysi, Johannes Haarer, Marcel Halama, Janine Haldemann, Pius Heer, Benjamin Heimgartner, Beat Helbling, Peter Hengstler, Denise Herzog, Cyrill Hess, Roxane Hessler, Klaas Heyland, Thomas Hinterleitner, Claudia Hirschi, Pascal Juillerat, Stephan Kayser, Céline Keller, Carolina Khalid-de Bakker, Christina Knellwolf(-Grieger), Christoph Knoblauch, Henrik Köhler, Rebekka Koller, Claudia Krieger(-Grübel), Patrizia Künzler, Rachel Kusche, Frank Serge Lehmann, Andrew J. Macpherson, Michel H. Maillard, Michael Manz, Astrid Marot, Rémy Meier, Christa Meyenberger, Pamela Meyer, Pierre Michetti, Benjamin Misselwitz, Patrick Mosler, Christian Mottet, Christoph Müller, Beat Müllhaupt, Leilla Musso, Michaela Neagu, Cristina Nichita, Andreas Nydegger, Nicole Obialo, Diana Ollo, Cassandra Oropesa, Ulrich Peter, Daniel Peternac, Laetitia Marie Petit, Valérie Pittet, Daniel Pohl, Marc Porzner, Claudia Preissler, Nadia Raschle, Ronald Rentsch, Sophie Restellini, Alexandre Restellini, Jean-Pierre Richterich, Frederic Ris, Branislav Risti, Marc Alain Ritz, Gerhard Rogler, Nina Röhrich, Jean-Benoît Rossel, Vanessa Rueger, Monica Rusticeanu, Markus Sagmeister, Gaby Saner, Bernhard Sauter, Mikael Sawatzki, Michael Scharl, Martin Schelling, Susanne Schibli, Hugo Schlauri, Dominique Schluckebier, Sybille Schmid(-Uebelhart), Daniela Schmid, Jean-François Schnegg, Alain Schoepfer, Vivianne Seematter, Frank Seibold, Mariam Seirafi, Gian-Marco Semadeni, Arne Senning, Christiane Sokollik, Joachim Sommer, Johannes Spalinger, Holger Spangenberger, Philippe Stadler, Peter Staub, Dominic Staudenmann, Volker Stenz, Michael Steuerwald, Alex Straumann, Bruno Strebel, Andreas Stulz, Michael Sulz, Aurora Tatu, Michela Tempia-Caliera, Amman Thomas, Joël Thorens, Kaspar Truninger, Radu Tutuian, Patrick Urfer, Stephan Vavricka, Francesco Viani, Jürg Vögtlin, Roland Von Känel, Dominique Vouillamoz, Rachel Vulliamy, Paul Wiesel, Reiner Wiest, Stefanie Wöhrle, Tina Wylie, Samuel Zamora, Silvan Zander, Jonas Zeitz, and Dorothee Zimmermann.

ACKNOWLEDGMENTS

This work is part of the Ph.D. thesis of B.K. Philippe Demougin (Biozentrum, Basel) and Christian Beisel (Genomics Facility Basel, ETH Zürich) helped with RNA-seq. Calculations were performed at the sciCORE (https://scicore.unibas.ch/) scientific computing center at the University of Basel. J.H.N. was supported by SNSF grants 310030_175548 and 316030_170809. The SNSF grant 31AC-0_198951 to J.H.N. financed the publication of our manuscript without restrictions (gold open access). T.K. was supported by SNSF M.D. Ph.D. fellowship 323530_183981. The Swiss IBD Cohort Investigators were supported by SNSF grant 33CS30-148422. E.J.V. was supported by grants from the Swedish Research Council VR grant K2015-68X-22765-01-6, Formas grant FR-2016/0005, Cancerfonden (19 0395 Pj), and the Wallenberg Academy Fellow program.

AUTHOR CONTRIBUTIONS

B.K., C.D., P.W., O.E.D., R.A.M., H.M., T.K., S.D., and C.K.A. performed experiments. P.H. provided patient samples, and P.P.H. provided *V. anguillarum* extracts. F.G. performed bioinformatics analysis of the RNA-seq data. Y.F. provided IBD patient statistics. E.J.V. and J.H.N. conceived the idea. B.K., C.D., E.J.V., and J.H.N. wrote the paper. All authors discussed the data and read and approved the manuscript.

DECLARATION OF INTERESTS

The authors declare no competing interests.

Received: August 5, 2019
Revised: March 23, 2020
Accepted: July 10, 2020
Published: August 4, 2020

REFERENCES

Bain, C.C., Scott, C.L., Uronen-Hansson, H., Gudjonsson, S., Jansson, O., Grip, O., Guilliams, M., Malissen, B., Agace, W.W., and Mowat, A.M. (2013). Resident and pro-inflammatory macrophages in the colon represent alternative context-dependent fates of the same Ly6Chi monocyte precursors. Mucosal Immunol. *6*, 498–510.

Bates, J.M., Mittge, E., Kuhlman, J., Baden, K.N., Cheesman, S.E., and Guillemin, K. (2006). Distinct signals from the microbiota promote different aspects of zebrafish gut differentiation. Dev. Biol. *297*, 374–386.

Bernardo, D., Marin, A.C., Fernández-Tomé, S., Montalban-Arques, A., Carrasco, A., Tristán, E., Ortega-Moreno, L., Mora-Gutiérrez, I., Díaz-Guerra, A., Caminero-Fernández, R., et al. (2018). Human intestinal pro-inflammatory CD11c^{high}CCR2^{+}CX3CR1^{+} macrophages, but not their tolerogenic CD11c^{-}CCR2^{-}CX3CR1^{-} counterparts, are expanded in inflammatory bowel disease. Mucosal Immunol. *11*, 1114–1126.

Bernshtein, B., Curato, C., Ioannou, M., Thaiss, C.A., Gross-Vered, M., Kolesnikov, M., Wang, Q., David, E., Chappell-Maor, L., Harmelin, A., et al. (2019). IL-23-producing IL-10Rα-deficient gut macrophages elicit an IL-22-driven proinflammatory epithelial cell response. Sci. Immunol. *4*, eaau6571.

Binti Mohd Amir, N.A.S., Mackenzie, A.E., Jenkins, L., Boustani, K., Hillier, M.C., Tsuchiya, T., Milligan, G., and Pease, J.E. (2018). Evidence for the Existence of a CXCL17 Receptor Distinct from GPR35. J. Immunol. *201*, 714–724.

Chen, H., Nwe, P.K., Yang, Y., Rosen, C.E., Bielecka, A.A., Kuchroo, M., Cline, G.W., Kruse, A.C., Ring, A.M., Crawford, J.M., and Palm, N.W. (2019). A Forward Chemical Genetic Screen Reveals Gut Microbiota Metabolites That Modulate Host Physiology. Cell *177*, 1217–1231.e18.

Cohen, L.J., Esterhazy, D., Kim, S.H., Lemetre, C., Aguilar, R.R., Gordon, E.A., Pickard, A.J., Cross, J.R., Emiliano, A.B., Han, S.M., et al. (2017). Commensal bacteria make GPCR ligands that mimic human signalling molecules. Nature *549*, 48–53.

Corazza, N., Eichenberger, S., Eugster, H.P., and Mueller, C. (1999). Nonlymphocyte-derived tumor necrosis factor is required for induction of colitis in recombination activating gene (RAG)2(-/-) mice upon transfer of CD4(+) CD45RB(hi) T cells. J. Exp. Med. *190*, 1479–1492.

Cullinane, M., Baysse, C., Morrissey, J.P., and O'Gara, F. (2005). Identification of two lysophosphatidic acid acyltransferase genes with overlapping function in Pseudomonas fluorescens. Microbiology *151*, 3071–3080.

Czarnewski, P., Parigi, S.M., Sorini, C., Diaz, O.E., Das, S., Gagliani, N., and Villablanca, E.J. (2019). Conserved transcriptomic profile between mouse and human colitis allows unsupervised patient stratification. Nat. Commun. *10*, 2892.

Dobin, A., Davis, C.A., Schlesinger, F., Drenkow, J., Zaleski, C., Jha, S., Batut, P., Chaisson, M., and Gingeras, T.R. (2013). STAR: ultrafast universal RNA-seq aligner. Bioinformatics *29*, 15–21.

Ellinghaus, D., Folseraas, T., Holm, K., Ellinghaus, E., Melum, E., Balschun, T., Laerdahl, J.K., Shiryaev, A., Gotthardt, D.N., Weismüller, T.J., et al. (2013). Genome-wide association analysis in primary sclerosing cholangitis and ulcerative colitis identifies risk loci at GPR35 and TCF4. Hepatology *58*, 1074–1083.

Farooq, S.M., Hou, Y., Li, H., O'Meara, M., Wang, Y., Li, C., and Wang, J.M. (2018). Disruption of GPR35 Exacerbates Dextran Sulfate Sodium-Induced Colitis in Mice. Dig. Dis. Sci. *63*, 2910–2922.

Gaidatzis, D., Lerch, A., Hahne, F., and Stadler, M.B. (2015). QuasR: quantification and annotation of short reads in R. Bioinformatics *31*, 1130–1132.

Gesta, S., Simon, M.F., Rey, A., Sibrac, D., Girard, A., Lafontan, M., Valet, P., and Saulnier-Blache, J.S. (2002). Secretion of a lysophospholipase D activity by adipocytes: involvement in lysophosphatidic acid synthesis. J. Lipid Res. *43*, 904–910.

Günther, C., Martini, E., Wittkopf, N., Amann, K., Weigmann, B., Neumann, H., Waldner, M.J., Hedrick, S.M., Tenzer, S., Neurath, M.F., and Becker, C. (2011). Caspase-8 regulates TNF-α-induced epithelial necroptosis and terminal ileitis. Nature *477*, 335–339.

Hanauer, S.B., Feagan, B.G., Lichtenstein, G.R., Mayer, L.F., Schreiber, S., Colombel, J.F., Rachmilewitz, D., Wolf, D.C., Olson, A., Bao, W., and Rutgeerts, P.; ACCENT I Study Group (2002). Maintenance infliximab for Crohn's disease: the ACCENT I randomised trial. Lancet *359*, 1541–1549.

Hernández, P.P., Strzelecka, P.M., Athanasiadis, E.I., Hall, D., Robalo, A.F., Collins, C.M., Boudinot, P., Levraud, J.P., and Cvejic, A. (2018). Single-cell transcriptional analysis reveals ILC-like cells in zebrafish. Sci. Immunol. *3*, eaau5265.

Imielinski, M., Baldassano, R.N., Griffiths, A., Russell, R.K., Annese, V., Dubinsky, M., Kugathasan, S., Bradfield, J.P., Walters, T.D., Sleiman, P., et al.; Western Regional Alliance for Pediatric IBD; International IBD Genetics Consortium; NIDDK IBD Genetics Consortium; Belgian-French IBD Consortium; Wellcome Trust Case Control Consortium (2009). Common variants at five new loci associated with early-onset inflammatory bowel disease. Nat. Genet. *41*, 1335–1340.

Lattin, J.E., Schroder, K., Su, A.I., Walker, J.R., Zhang, J., Wiltshire, T., Saijo, K., Glass, C.K., Hume, D.A., Kellie, S., and Sweet, M.J. (2008). Expression analysis of G Protein-Coupled Receptors in mouse macrophages. Immunome Res. *4*, 5.

Li, M., Zhao, L., Page-McCaw, P.S., and Chen, W. (2016). Zebrafish Genome Engineering Using the CRISPR-Cas9 System. Trends Genet. *32*, 815–827.

Lin, Z., Li, S., Feng, C., Yang, S., Wang, H., Ma, D., Zhang, J., Gou, M., Bu, D., Zhang, T., et al. (2016). Stabilizing mutations of KLHL24 ubiquitin ligase cause loss of keratin 14 and human skin fragility. Nat. Genet. *48*, 1508–1516.

MacDonald, T.T., Monteleone, I., Fantini, M.C., and Monteleone, G. (2011). Regulation of homeostasis and inflammation in the intestine. Gastroenterology *140*, 1768–1775.

Mackenzie, A.E., Lappin, J.E., Taylor, D.L., Nicklin, S.A., and Milligan, G. (2011). GPR35 as a Novel Therapeutic Target. Front. Endocrinol. (Lausanne) *2*, 68.

Maravillas-Montero, J.L., Burkhardt, A.M., Hevezi, P.A., Carnevale, C.D., Smit, M.J., and Zlotnik, A. (2015). Cutting edge: GPR35/CXCR8 is the receptor of the mucosal chemokine CXCL17. J. Immunol. *194*, 29–33.

McCarthy, D.J., Chen, Y., and Smyth, G.K. (2012). Differential expression analysis of multifactor RNA-Seq experiments with respect to biological variation. Nucleic Acids Res. *40*, 4288–4297.

Melhem, H., Spalinger, M.R., Cosin-Roger, J., Atrott, K., Lang, S., Wojtal, K.A., Vavricka, S.R., Rogler, G., and Frey-Wagner, I. (2017). Prdx6 Deficiency Ameliorates DSS Colitis: Relevance of Compensatory Antioxidant Mechanisms. J. Crohn's Colitis *11*, 871–884.

Milligan, G. (2018). G protein-coupled receptors not currently in the spotlight: free fatty acid receptor 2 and GPR35. Br. J. Pharmacol. *175*, 2543–2553.

Mirzoyan, K., Denis, C., Casemayou, A., Gilet, M., Marsal, D., Goudounéche, D., Faguer, S., Bascands, J.L., Schanstra, J.P., and Saulnier-Blache, J.S. (2017). Lysophosphatidic Acid Protects Against Endotoxin-Induced Acute Kidney Injury. Inflammation *40*, 1707–1716.

Mizoguchi, E., Hachiya, Y., Kawada, M., Nagatani, K., Ogawa, A., Sugimoto, K., Mizoguchi, A., and Podolsky, D.K. (2008). TNF receptor type I-dependent activation of innate responses to reduce intestinal damage-associated mortality. Gastroenterology *134*, 470–480.

Naito, Y., Takagi, T., Handa, O., Ishikawa, T., Nakagawa, S., Yamaguchi, T., Yoshida, N., Minami, M., Kita, M., Imanishi, J., and Yoshikawa, T. (2003). Enhanced intestinal inflammation induced by dextran sulfate sodium in tumor necrosis factor-alpha deficient mice. J. Gastroenterol. Hepatol. *18*, 560–569.

Neurath, M.F., Fuss, I., Pasparakis, M., Alexopoulou, L., Haralambous, S., Meyer zum Büschenfelde, K.H., Strober, W., and Kollias, G. (1997). Predominant pathogenic role of tumor necrosis factor in experimental colitis in mice. Eur. J. Immunol. *27*, 1743–1750.

Nguyen-Chi, M., Laplace-Builhe, B., Travnickova, J., Luz-Crawford, P., Tejedor, G., Phan, Q.T., Duroux-Richard, I., Levraud, J.P., Kissa, K., Lutfalla, G., et al. (2015). Identification of polarized macrophage subsets in zebrafish. eLife *4*, e07288.

Noti, M., Corazza, N., Mueller, C., Berger, B., and Brunner, T. (2010). TNF suppresses acute intestinal inflammation by inducing local glucocorticoid synthesis. J. Exp. Med. *207*, 1057–1066.

Oh, Y.S., Heo, K., Kim, E.K., Jang, J.H., Bae, S.S., Park, J.B., Kim, Y.H., Song, M., Kim, S.R., Ryu, S.H., et al. (2017). Dynamic relocalization of NHERF1 mediates chemotactic migration of ovarian cancer cells toward lysophosphatidic acid stimulation. Exp. Mol. Med. *49*, e351.

Oka, S., Ota, R., Shima, M., Yamashita, A., and Sugiura, T. (2010). GPR35 is a novel lysophosphatidic acid receptor. Biochem. Biophys. Res. Commun. *395*, 232–237.

Pittet, V., Juillerat, P., Mottet, C., Felley, C., Ballabeni, P., Burnand, B., Michetti, P., and Vader, J.P.; Swiss IBD Cohort Study Group (2009). Cohort profile: the Swiss Inflammatory Bowel Disease Cohort Study (SIBDCS). Int. J. Epidemiol. *38*, 922–931.

Plastira, I., Bernhart, E., Goeritzer, M., DeVaney, T., Reicher, H., Hammer, A., Lohberger, B., Wintersperger, A., Zucol, B., Graier, W.F., et al. (2017). Lysophosphatidic acid via LPA-receptor 5/protein kinase D-dependent pathways induces a motile and pro-inflammatory microglial phenotype. J. Neuroinflammation *14*, 253.

Present, D.H., Rutgeerts, P., Targan, S., Hanauer, S.B., Mayer, L., van Hogezand, R.A., Podolsky, D.K., Sands, B.E., Braakman, T., DeWoody, K.L., et al. (1999). Infliximab for the treatment of fistulas in patients with Crohn's disease. N. Engl. J. Med. *340*, 1398–1405.

Radulovic, K., Ayata, C.K., Mak'Anyengo, R., Lechner, K., Wuggenig, P., Kaya, B., Hruz, P., Gomez de Agüero, M., Broz, P., Weigmann, B., and Niess, J.H. (2019). NLRP6 Deficiency in CD4 T Cells Decreases T Cell Survival Associated with Increased Cell Death. J. Immunol. *203*, 544–556.

Reinecker, H.C., Steffen, M., Witthoeft, T., Pflueger, I., Schreiber, S., MacDermott, R.P., and Raedler, A. (1993). Enhanced secretion of tumour necrosis factor-alpha, IL-6, and IL-1 beta by isolated lamina propria mononuclear cells from patients with ulcerative colitis and Crohn's disease. Clin. Exp. Immunol. *94*, 174–181.

Rossini, V., Zhurina, D., Radulovic, K., Manta, C., Walther, P., Riedel, C.U., and Niess, J.H. (2014). CX3CR1^{+} cells facilitate the activation of CD4 T cells in the colonic lamina propria during antigen-driven colitis. Mucosal Immunol. *7*, 533–548.

Sands, B.E., Tremaine, W.J., Sandborn, W.J., Rutgeerts, P.J., Hanauer, S.B., Mayer, L., Targan, S.R., and Podolsky, D.K. (2001). Infliximab in the treatment of severe, steroid-refractory ulcerative colitis: a pilot study. Inflamm. Bowel Dis. *7*, 83–88.

Schneditz, G., Elias, J.E., Pagano, E., Zaeem Cader, M., Saveljeva, S., Long, K., Mukhopadhyay, S., Arasteh, M., Lawley, T.D., Dougan, G., et al. (2019).

GPR35 promotes glycolysis, proliferation, and oncogenic signaling by engaging with the sodium potassium pump. Sci. Signal. *12*, eaau9048.

Serbina, N.V., and Pamer, E.G. (2006). Monocyte emigration from bone marrow during bacterial infection requires signals mediated by chemokine receptor CCR2. Nat. Immunol. *7*, 311–317.

Shouval, D.S., Biswas, A., Goettel, J.A., McCann, K., Conaway, E., Redhu, N.S., Mascanfroni, I.D., Al Adham, Z., Lavoie, S., Ibourk, M., et al. (2014). Interleukin-10 receptor signaling in innate immune cells regulates mucosal immune tolerance and anti-inflammatory macrophage function. Immunity *40*, 706–719.

Siegel, S.A., Shealy, D.J., Nakada, M.T., Le, J., Woulfe, D.S., Probert, L., Kollias, G., Ghrayeb, J., Vilcek, J., and Daddona, P.E. (1995). The mouse/human chimeric monoclonal antibody cA2 neutralizes TNF in vitro and protects transgenic mice from cachexia and TNF lethality in vivo. Cytokine *7*, 15–25.

Southern, C., Cook, J.M., Neetoo-Isseljee, Z., Taylor, D.L., Kettleborough, C.A., Merritt, A., Bassoni, D.L., Raab, W.J., Quinn, E., Wehrman, T.S., et al. (2013). Screening β-arrestin recruitment for the identification of natural ligands for orphan G-protein-coupled receptors. J. Biomol. Screen. *18*, 599–609.

Souza, A.L., Fiorini Aguiar, S.L., Gonçalves Miranda, M.C., Lemos, L., Freitas Guimaraes, M.A., Reis, D.S., Vieira Barros, P.A., Veloso, E.S., Carvalho, T.G., Ribeiro, F.M., et al. (2017). Consumption of Diet Containing Free Amino Acids Exacerbates Colitis in Mice. Front. Immunol. *8*, 1587.

Steinert, A., Linas, I., Kaya, B., Ibrahim, M., Schlitzer, A., Hruz, P., Radulovic, K., Terracciano, L., Macpherson, A.J., and Niess, J.H. (2017). The Stimulation of Macrophages with TLR Ligands Supports Increased IL-19 Expression in Inflammatory Bowel Disease Patients and in Colitis Models. J. Immunol. *199*, 2570–2584.

Takeda, Y., Matoba, K., Kawanami, D., Nagai, Y., Akamine, T., Ishizawa, S., Kanazawa, Y., Yokota, T., and Utsunomiya, K. (2019). ROCK2 Regulates Monocyte Migration and Cell to Cell Adhesion in Vascular Endothelial Cells. Int. J. Mol. Sci. *20*, 1331.

Targan, S.R., Hanauer, S.B., van Deventer, S.J., Mayer, L., Present, D.H., Braakman, T., DeWoody, K.L., Schaible, T.F., and Rutgeerts, P.J. (1997). A short-term study of chimeric monoclonal antibody cA2 to tumor necrosis factor alpha for Crohn's disease. Crohn's Disease cA2 Study Group. N. Engl. J. Med. *337*, 1029–1035.

Tsukahara, T., Hamouda, N., Utsumi, D., Matsumoto, K., Amagase, K., and Kato, S. (2017). G protein-coupled receptor 35 contributes to mucosal repair in mice via migration of colonic epithelial cells. Pharmacol. Res. *123*, 27–39.

Uchimura, Y., Fuhrer, T., Li, H., Lawson, M.A., Zimmermann, M., Yilmaz, B., Zindel, J., Ronchi, F., Sorribas, M., Hapfelmeier, S., et al. (2018). Antibodies Set Boundaries Limiting Microbial Metabolite Penetration and the Resultant Mammalian Host Response. Immunity *49*, 545–559.e5.

Wang, J., Simonavicius, N., Wu, X., Swaminath, G., Reagan, J., Tian, H., and Ling, L. (2006). Kynurenic acid as a ligand for orphan G protein-coupled receptor GPR35. J. Biol. Chem. *281*, 22021–22028.

Wirtz, S., Neufert, C., Weigmann, B., and Neurath, M.F. (2007). Chemically induced mouse models of intestinal inflammation. Nat. Protoc. *2*, 541–546.

Wuggenig, P., Kaya, B., Melhem, H., Ayata, C.K., Hruz, P., Sayan, A.E., Tsumura, H., Ito, M., Roux, J., and Niess, J.H.; Swiss IBD Cohort Investigators (2020). Loss of the branched-chain amino acid transporter CD98hc alters the development of colonic macrophages in mice. Commun. Biol. *3*, 130.

Ye, X., and Chun, J. (2010). Lysophosphatidic acid (LPA) signaling in vertebrate reproduction. Trends Endocrinol. Metab. *21*, 17–24.

Zigmond, E., Bernshtein, B., Friedlander, G., Walker, C.R., Yona, S., Kim, K.W., Brenner, O., Krauthgamer, R., Varol, C., Müller, W., and Jung, S. (2014). Macrophage-restricted interleukin-10 receptor deficiency, but not IL-10 deficiency, causes severe spontaneous colitis. Immunity *40*, 720–733.

STAR★METHODS

KEY RESOURCES TABLE

REAGENT or RESOURCE	SOURCE	IDENTIFIER
Antibodies		
Anti-mouse/human CD16/CD32 monoclonal antibody (clone 93)	Invitrogen	Cat# 14-0161-85; RRID: AB_467134
Anti-mouse CD4- BV510 (clone RM4-5)	BioLegend	Cat# 100559; RRID: AB_2562608
Anti-mouse CD45- eVolve655 (clone 30-F11)	eBioscience	Cat# 62-0451-82; RRID: AB_2744774
Anti-mouse CD19- BV785 (clone 6D5)	BioLegend	Cat# 115543; RRID: AB_11218994
Anti-mouse CD11b- FITC (clone M1/70)	BioLegend	Cat# 101206; RRID: AB_312789
Anti-mouse CD8a- PerCP (clone 53-6.7)	BioLegend	Cat#100732; RRID: AB_893423
Anti-mouse Ly-6C- PerCP/Cy5.5 (clone HK1.4)	BioLegend	Cat# 128011; RRID: AB_1659242
Anti-mouse CD64- PE/Cy7 (clone X54-5/7.1)	BioLegend	Cat# 139314; RRID: AB_2563904
Anti-mouse Ly-6G- APC (clone 1A8)	BioLegend	Cat# 127613; RRID: AB_1877163
Anti-mouse CD3- Alexa Fluor 700 (clone 17A2)	BioLegend	Cat# 100216; RRID: AB_493697
Anti-mouse I-A/I-E (MHC-II) – Alexa Fluor 700 (clone M5/114.15.2)	BioLegend	Cat# 107622; RRID: AB_493727
Anti-mouse CD45- APC/Cy7 (clone 30-F11)	BioLegend	Cat# 103115; RRID: AB_312980
Anti-mouse CD11c- APC/Fire750 (clone N418)	BioLegend	Cat# 117352; RRID: AB_2572124
Anti-mouse CD3- Biotin (clone 145-2C11)	BioLegend	Cat# 100303; RRID: AB_312668
Anti-mouse CD19- Biotin (clone 6D5)	BioLegend	Cat# 115503; RRID: AB_313638
Anti-mouse NK1.1- Biotin (clone PK136)	BioLegend	Cat# 115503; RRID: AB_313638
Anti-mouse CD8a- Biotin (clone 53-6.7)	BioLegend	Cat# 100703; RRID: AB_312742
CD8-PerCP (Clone 53-6.7)	BioLegend	Cat# 100732; RRID: AB_893423
CD8-PerCP/Cy5.5 (Clone 53-6.7)	BioLegend	Cat# 100734; RRID: AB_2075238
Streptavidin- eFluor450	eBioscience	Cat# 48-4317-82; RRID: AB_10359737
Rabbit Anti-mouse/human GPR35	Novus Biologicals	Cat# NBP2-24640; RRID: N/A
Goat Anti-Rabbit IgG (H+L) Alexa Fluor 647	Invitrogen	Cat# A-21244; RRID: AB_141663
Anti-mouse CD90.2- APC/Cy7 (clone 30-H12)	BioLegend	Cat# 105327; RRID: AB_10613280
Anti-mouse CD11c- Biotin (clone N418)	BioLegend	Cat# 117303; RRID: AB_313772
Anti-mouse B220- Biotin (clone RA3-6B2)	BD Biosciences	Cat# 553085; RRID: AB_394615
Anti-mouse Ly-6G/Ly-6C (Gr-1) (clone RB6-8C5)	BioLegend	Cat# 108403; RRID: AB_313368
Anti-mouse TCR β chain- Biotin (clone H57-597)	BioLegend	Cat# 109203; RRID: AB_313426
Anti-mouse TCR γ/δ- Biotin (clone GL3)	BioLegend	Cat# 118103; RRID: AB_313827
Anti-mouse TER-119- Biotin (clone TER-119)	BioLegend	Cat# 116203; RRID: AB_313704
Anti- mouse GATA3- APC (clone 16E10A23)	BioLegend	Cat# 653805; RRID: AB_2562724
Anti-mouse RORγt- PerCP- Cy™5.5 (clone Q31-378)	BD Biosciences	Cat# 562683; RRID: AB_2737720
Anti-mouse T-bet- PE/Cy7 (clone 4B10)	BioLegend	Cat# 644823; RRID: AB_2561760
Anti-mouse NKp46- BV421 (clone 29A1.4)	BioLegend	Cat# 137611; RRID: AB_10915472
Anti-human/mouse EOMES- FITC (clone WD1928)	Invitrogen	Cat# 11-4877-42; RRID: AB_2572499
anti- human/mouse ENPP2 (autotaxin) (clone 1F8)	Abcam	Cat# ab77104; RRID: AB_2041145
Rabbit anti- p44/42 MAPK (Erk1/2) (clone 137F5)	Cell Signaling Technology	Cat# 4695; RRID: AB_390779
Rabbit Phospho-p44/42 MAPK (Erk1/2) (Thr202/Tyr204) (clone D13.14.4E)	Cell Signaling Technology	Cat# 4370; RRID: AB_2315112
Rabbit anti- NF-κB p65 (clone D14E12)	Cell Signaling Technology	Cat# 8242; RRID: AB_10859369
Rabbit anti- NF-κB p65 phospho (Ser536) (clone 93H1)	Cell Signaling Technology	Cat# 3033; RRID: AB_331284
Mouse anti-STAT3 (clone 124H6)	Cell Signaling Technology	Cat# 9139; RRID: AB_331757

(*Continued on next page*)

Continued

REAGENT or RESOURCE	SOURCE	IDENTIFIER
Rabbit anti- phospho-STAT3 (Tyr705) (clone D3A7)	Cell Signaling Technology	Cat# 9145; RRID: AB_2491009
Mouse anti- Actin (clone C4)	BD Biosciences	Cat# 612656; RRID: AB_2289199
Peroxidase-AffiniPure Goat Anti-Rabbit IgG (H+L)	Jackson ImmunoResearch	Cat# 111-035-144; RRID: AB_2307391
Peroxidase-AffiniPure Goat Anti-Mouse IgG (H+L)	Jackson ImmunoResearch	Cat# 115-035-146; RRID: AB_2307392
Bacterial and Virus Strains		
E.coli DH10B pCFP-OVA	Rossini et al., 2014	N/A
Vibrio anguillarum strain 1669	Hernández et al., 2018	N/A
Biological Samples		
Human IBD intestinal biopsies for RNA	Swiss IBD cohort	N/A
Human IBD intestinal biopsies for GPR35 staining	Basel IBD cohort	N/A
Chemicals, Peptides, and Recombinant Proteins		
Tamoxifen	MP Biomedicals	Cat# 0215673891; CAS: 10540-29-1
Corn oil	Sigma-Aldrich	Cat# C8267; CAS: 8001-30-7
Dextran sulfate sodium salt	MP Biomedicals	Cat# 0216011001; CAS: 9011-18-1
Ethylenediaminetetraacetic acid (EDTA)	Sigma-Aldrich	Cat# EDS; CAS: 60-00-4
Triton® X 100	Roth	Cat# 3051
TRI Reagent®	Sigma-Aldrich	Cat# T9424; MDL: MFCD00213058
Collagenase from *Clostridium histolyticum* Type VIII	Sigma-Aldrich	Cat# 2139; CAS: 9001-12-1
DNase I recombinant	Roche	Cat# 04536282001; CAS: 9003-98-9
Recombinant mouse M-CSF	Biolegend	Cat# 576406
Oleoyl-L-α-lysophosphatidic acid sodium salt	Sigma-Aldrich	Cat# L7260; CAS: 22556-62-3
Lipopolysaccharides from *Escherichia coli* O111:B4	Sigma-Aldrich	Cat# L2630; MDL: MFCD00164401
Fixable Fixable Viability Dye eFluor 455UV	Invitrogen	Cat# 65-0868-18
Fluorescein isothiocyanate (FITC)–dextran	Sigma-Aldrich	Cat# 46944; CAS: 60842-46-8
2,4,6-Trinitrobenzenesulfonic acid (TNBS)	Sigma-Aldrich	Cat# P2297; CAS: 2508-19-2
Critical Commercial Assays		
Direct-zol™ RNA Miniprep Kit	Zymo Research	Cat# R2052
QuantiNova SYBR Green PCR Kit	QIAGEN	Cat# 208052
cAMP Hunter™ eXpress GPR35 CHO-K1 GPCR assay	DiscoverX	Cat# 95-0152E2CP
High Capacity cDNA Reverse Transcription	Applied Biosystems	Cat# 4368813
LEGENDplex™ bead-based immunoassay	Biolegend	N/A (custom panel)
SuperSignal West Femto Maximum Sensitivity Substrate	Thermo Scientific	Cat# 34095
SuperSignal™ West Pico PLUS Chemiluminescent Substrate	Thermo Scientific	Cat# 34580
Deposited Data		
Low input RNA sequencing of GPR35-positive and negative intestinal macrophages	This paper	GEO: GSE131858
GPR35 mediates lysophosphatidic acid-signaling in bone marrow-derived macrophages at the transcriptional level	This paper	GEO: GSE153012
Experimental Models: Organisms/Strains		
Mouse: C57BL/6NCrl	Charles River Laboratories	RRID: IMSR_CRL:027
Mouse: Cx3cr1-GFP: B6.129P-Cx3cr1$^{tm1Litt/J}$	The Jackson Laboratory	RRID: IMSR_JAX:005582
Mouse: Cx3cr1-CreER: B6.129P2(Cg)-Cx3cr1$^{tm2.1(cre/ERT2)Litt}$/WganJ	The Jackson Laboratory	RRID: IMSR_JAX:021160
Mouse: Gpr35-tdTomato: Gpr35 < tm1.1Niess >	Mouse Genome Informatics Jackson Laboratory	MGI:6436879
Mouse: Gpr35$^{-/-}$: Gpr35 < em1Niess >	Mouse Genome Informatics Jackson Laboratory	MGI:6436880

(*Continued on next page*)

Continued

REAGENT or RESOURCE	SOURCE	IDENTIFIER
Mouse: Gpr35-flox: Gpr35 < em2Niess >	Mouse Genome Informatics Jackson Laboratory	MGI:6436881
Mouse: C57BL/6 (GF)	Core Facility for Germ-Free Research, Karolinska Institutet	N/A
Zebrafish: Tg(mpeg1:mCherry)	(Nguyen-Chi et al., 2015)	ZDB-FISH-151214-3
Zebrafish: gpr35b^{uu1892}	Genome Engineering Zebrafish, Science for Life Laboratory (SciLifeLab)	ZDB-ALT-200624-3
Oligonucleotides		
Primers for qRT-PCR and genotyping, see Table S1	This paper	N/A
Software and Algorithms		
FlowJo version 10.5.3	Tree Star Inc.	https://www.flowjo.com/
GraphPad Prism version 7.03	GraphPad Software Inc.	https://www.graphpad.com/
ImageJ	ImageJ.Ink	https://imagej.net/Welcome
NIS- Elements Confocal Software AR	Nikon Instruments Inc.	https://www.microscope.healthcare.nikon.com/products/software/nis-elements/nis-elements-advanced-research
Other		
Sequencing data for *atx* expression in the colon of mice with DSS colitis	(Czarnewski et al., 2019)	N/A

RESOURCE AVAILABILITY

Lead Contact

Further information and requests for resources and reagents should be directed to and will be fulfilled by Eduardo J. Villablanca (eduardo.villablanca@ki.se).

Materials Availability

Zebrafish and mouse lines generated in this study have been deposited to ZFIN and the Mouse Genome Informatics (MGI), respectively. Please see the Key Resources Table for detailed information.

Data and Code Availability

The datasets generated during this study are available at Gene Expression Omnibus (GEO) with accession codes GEO: GSE131858 for SmartSeq4 of colonic macrophages, and GEO: GSE153012 for TrueSeq of BMDMs.

EXPERIMENTAL MODEL AND SUBJECT DETAILS

Mouse lines

C57BL/6, *Rag2*$^{-/-}$, *Cx3cr1*-GFP (B6.129P-Cx3cr1$^{tm1Litt/J}$) and Cx3cr1^{CreER} (B6.129P2(Cg)-*Cx3cr1*$^{tm2.1(cre/ERT2)Litt/WganJ}$) mice were bred and maintained in the animal facility of Department of Biomedicine, University of Basel, Switzerland or the respective facility at the Karolinska Institutet, Solna, Sweden. *Gpr35*-tdTomato, *Gpr35*$^{-/-}$ and *Gpr35*$^{flox/flox}$ animals were constructed as described below. *Gpr35*-tdTomato mice were crossed with *Cx3cr1*-GFP mice to generate double reporter mice, and *Gpr35*$^{flox/flox}$ were crossed with *Cx3cr1*^{CreER} to obtain *Gpr35*$^{\Delta CX3CR1}$ mice, in which the tamoxifen-inducible, Cre-mediated recombination will lead to the excision of GPR35 in CX3CR1^{+} cells. All animals were kept under specific pathogen-free (SPF) conditions. Germ-free C57BL/6 mice were obtained from the Core Facility for Germ-Free Research at the Karolinska Institutet, Solna, Sweden. For *in vivo* and *in vitro* experiments at least 3 mice per group were included. Animals between 6-12 weeks of age were randomly selected for experimental groups. All mouse experiments were conducted under the Swiss Federal and Cantonal regulations (animal protocol number 2832 (canton Basel-Stadt)) and the Stockholm regional ethics committee under approved ethical number N89-15.

Generation of Gpr35-IRES-tdTomato knock-in mice

Gpr35-IRES-tdTomato knock-in mouse line was generated by Biocytogen (Wakefiled, USA) by introducing IRES-tdTomato between the protein-coding sequences of the targeted gene and 3′UTR under the genetic background of C57BL/6J. In brief, for construction

of the targeting vector, 4.7-kb left homology arm spanning exon 1 and an FRT-flanked neo cassette were inserted 352bp upstream of exon 2; an internal ribosome entry site 2 (IRES2) sequence (allows translation initiation in the middle of an mRNA sequence), a tdTomato reporter and 3.9-kb right homology arm were inserted just downstream of the stop codon. The complete sequence of the targeting vector was verified by sequencing analysis. After linearization, the targeting vector was transfected into C57BL/6J embryonic stem (ES) cells by electroporation. Eight positive ES clones were identified by Southern blot analysis with 5′probe and 3′probe, and Karyotype analysis. Positive ES clones were injected into BALB/c blastocysts and implanted into pseudopregnant females. Four chimeric male mice were crossed with FLP females to obtain F1 mice carrying the recombined allele with the removal of Neo selection cassette. The F1 mice were validated for germinal line transmission of the recombination event by using the PCR strategy. The elimination of the neo cassette in the offspring was analyzed by PCR with the primers Frt-F2 and Frt-R2 (Table S1). Male and female heterozygous mice were crossed to produce homozygous mutant mice. Reporter animals were genotyped by PCR with primers listed in Table S1. Following PCR cycling parameters were used with 35 cycles of amplification: denaturation 95°C for 2 min; amplification 95°C 30 s, 62°C 30 s, 72°C 25 s; final elongation 72°C 10 min.

Generation of Gpr35-flox and knock-out (KO) mice

Gpr35^{flox} and *Gpr35*$^{-/-}$ mice were generated using the CRISPR/Cas9 system by Biocytogen (Wakefiled, USA). Briefly, the Cas9/guide RNA (gRNA) target sequences were designed to the regions upstream of exon2 and downstream of 3′UTR. The targeting construct of *Gpr35*^{flox} consisting of 1.3 kb arms of homologous genomic sequence immediately upstream (5′) of exon 2 and downstream (3′) of 3′UTR flanked by two loxP sites (Figure S3A). Cas9 mRNA and sgRNAs were transcribed with T7 RNA polymerase *in vitro*. Cas9 mRNA, sgRNAs and donor vector were mixed at different concentrations and co-injected into the cytoplasm of fertilized eggs at the one-cell stage. The genotypes for *Gpr35*^{flox} and *Gpr35*$^{-/-}$ mice were validated by PCR amplification and direct sequencing. *Gpr35*^{flox} mice were further validated by Southern blot analysis.

For *Gpr35* targeting, two sgRNAs were designed to target the regions upstream of exon 2 and downstream of 3′UTR. For each targeted site, candidate sgRNAs were designed using the CRISPR design tool (https://www.sanger.ac.uk/htgt/wge/). sgRNAs were screened for on-target activity using the UCA kit (Lin et al., 2016). Cas9 mRNA and sgRNAs were transcribed with T7 RNA polymerase *in vitro*. For Cas9 mRNA and sgRNA production, the T7 promoter sequence was added to the Cas9 and sgRNA templates by PCR amplification. T7-Cas9 and T7-sgRNA PCR products were gel purified and used as the template for *in vitro* transcription with the MEGAshortscript T7 kit (Life Technologies) according to the kit protocol. Cas9 mRNA and sgRNAs were purified using the MEGAclear kit and eluted with Rnase-free water. The targeting construct of Gpr35 flox consisting of 1.3 kb arms of homologous genomic sequence immediately upstream (5′) of exon 2 and downstream (3′) of 3′UTR flanked by two loxP sites (Figure S3C). The donor vector was prepared using an endotoxin-free plasmid DNA kit. C57BL/6N females were used as embryo donors and pseudopregnant foster mothers. Superovulated C57BL/6N mice (3-4 weeks old) were mated to C57BL/6N stud males, and fertilized embryos were collected from the ampullae. Cas9 mRNA, sgRNAs and donor vector were mixed at different concentrations and co-injected into the cytoplasm of fertilized eggs at the one-cell stage. After injection, surviving zygotes were transferred into the oviducts of KM pseudopregnant females. The genotyping of *Gpr35*-deficient animals was done by PCR in 2 different reactions using the listed primers (Table S1) under the following conditions: initial denaturation at 95°C for 3 min; 35 cycles of denaturation 95°C 30 s, annealing 64°C 30 s, elongation 72°C 45 s; and final elongation 72°C 10 min. The *Gpr35*-flox mice were genotyped by PCR (for primers see Table S1) by denaturating at 95°C for 3 min, amplifying 35 cycles at 95°C 30 s, 62°C 30 s, 72°C 35 s and elongating at 72°C for 10 min.

Zebrafish lines

The *Tg(mpeg1:mCherry)* was kindly provided by Professor Georges Luftalla (Montpellier, France). The zebrafish predicted gene G-protein coupled receptor 35-like (LOC101882856) (mRNA sequence ID: XM_021466387.1, previous Ensembl ID: ENSDARG00000075877, current Ensembl ID: ENSDARG00000113303) was targeted using a CRISPR-Cas9 approach by the Genome Engineering Zebrafish, Science for Life Laboratory (SciLifeLab), Uppsala, Sweden. CRISPR/Cas9 gene editing was performed as previously described (Li et al., 2016) and the gRNA was targeted within exon 2 in the reverse strand with a gene specific gRNA-target sequence followed by a protospacer adjacent motif (Serbina and Pamer, 2006), (5′ GGT AGG CCA CAC GCT CAA ACA GG 3′ – PAM sequence is underlined). Eggs from WT AB strain were co-injected with a total volume of 2nL consisting of a mix of 300 pg Cas9 mRNA and 25pg of sgRNA at the single-cell stage. Founder screening by somatic activity test (CRISPR-STAT) and germline transmission were assayed using fluorescence PCR as previously described (Li et al., 2016). Briefly, injection groups with somatic activity were grown to adulthood for founder screening and positively identified founders (F_0) were in-crossed with another founder to screen for germline transmission in F_1 embryos. F_1 embryos were raised to adulthood, fin clipped and genotyped using fluorescence PCR followed by subsequent validation of the mutation using Sanger sequencing. F_1 heterozygotes were outcrossed with AB fish and the resulting F_2 heterozygotes were further maintained and in-crossed. The F_3 embryos were raised to adulthood and screened for homozygous mutants and wild-type zebrafish by PCR based genotyping (WT forward primer: 5′- TAG CCT GTT TGA GCG TGT GG-3′; mutant forward primer: 5′- CCA TTA GCC TGT GGC CT −3′; common reverse primer: 5′-CAC CAG CGA TTT GGT CAG AA-3′), which were further in-crossed (i.e., 'mutant with mutant' and 'wild-type with wild-type') to generate mutant and WT embryos that were subsequently used for experiments. For the purpose of experiments, the mating was performed in a random fashion at all occasions. For husbandry, embryos were kept and raised to adulthood in systems with circulating, filtered and temperature (28.5°C) controlled water. All procedures were performed according to Swedish and European regulations and

have been approved by the Uppsala University Ethical Committee for Animal Research (C161.14) and Karolinska Institutet Ethical Committee for Animal Research (N5756/17).

Primers used for fluorescence PCR

Forward M13F-tailed primer: 5′-TGT AAA ACG ACG GCC AGT CTC AAG CAA ACT GCT TCC TCT T-3′; Reverse PIG-tailed primer: 5′- GTG TCT TGC ATG TAG ATG TGA GTG TCG GT-3′; M13F FAM primer: /56FAM/ TGT AAA ACG ACG GCC AGT

Human inflammatory bowel disease biopsies

The study population for mRNA analysis included 31 patients with Crohn's disease and 31 patients with ulcerative colitis (20 with active disease, 11 in remission) recruited to Swiss Inflammatory Bowel Disease Cohort Study (SwissIBD cohort project 2016-12) (see Swiss IBD Cohort Investigators) started in 2006 (Pittet et al., 2009). The diagnoses of Crohn's disease and ulcerative colitis were validated by endoscopy, radiology or surgery at least 4 months before recruitment of the patients. Patients with colitis or ileitis caused by other conditions or with no permanent residency in Switzerland were excluded from the study. Ileocolonoscopy was done to confirm quiescent IBD or to determine the activity in active IBD. For active IBD, biopsies were taken from macroscopically inflamed regions. Table S2 gives detailed depiction of patient information. After the collection, the biopsies were kept in RNAlater® stabilization solution (Invitrogen) at −80°C until further use. The study population for immunofluorescence involved 4 ulcerative colitis and 3 Crohn's disease patients recruited to the Basel IBD cohort. The biopsies were taken from inflamed or non-inflamed regions of the same patients following ileocolonoscopy. The specimens were embedded in optimal cutting temperature (OCT) compound (Tissue-Tek) and stored at −80°C. Table S3 shows the detailed patient characteristics (ethics protocol EKBB 139/13 (PB 2016.02242) (Ethics Committee for Northwest and Central Switzerland (EKNZ).

METHOD DETAILS

Dextran sodium sulfate induced colitis mouse model

Weight-matched 6 to 12-week-old female mice were administered with 1.5%–2.5% DSS (MP Biomedicals) in the drinking water for 5 days followed by 2 days of normal drinking water. Mice were daily weighed and monitored for clinical colitis score. Clinical colitis scores were calculated according to the following criteria (Steinert et al., 2017): rectal bleeding: 0 - absent, 1 - bleeding; stool consistency: 0 - normal, 1 - loose stools, 2 - diarrhea; position: 0 - normal movement, 1 - reluctant to move, 2 - hunched back; fur: 0 - normal, 1 - ruffled, 2 - spiky; weight loss: 0 – no loss, 1 - bodyweight loss 0%–5%, 2 - bodyweight loss > 5 - 10%, 3 - bodyweight loss > 10 - 15%, 4 - bodyweight loss > 15%. Endpoints of the experiment are total score of $\geq$ 6, > 15% bodyweight loss, excessive bleeding, and rectal prolapse.

Hematoxylin-eosin (H&E) staining and histological scoring

5 μm paraffin sections from mouse colon were stained with H&E. Histological scores for colonic inflammation were assessed semi-quantitatively using the following criteria (Souza et al., 2017; Steinert et al., 2017): mucosal architecture (0:normal, 1-3: mild-extensive damage); cellular infiltration (0:normal, 1-3: mild-transmural); goblet cell depletion (0:no, 1:yes); crypt abscesses (0:no, 1:yes); extend of muscle thickening (0: normal, 1-3: mild-extensive). Tissues were scored by at least two blinded investigators and data is presented by the mean.

Mouse Endoscopy

To assess macroscopic colitis severity, mice were anaesthetized with 100 mg/kg bodyweight ketamine and 8 mg/kg bodyweight Xylazine intraperitoneally. The distal 3 cm of the colon and the rectum were examined with a Karl Storz Tele Pack Pal 20043020 (Karl Storz Endoskope, Tuttlingen, Germany) as previously described (Melhem et al., 2017).

Treatment of zebrafish with 2,4,6-Trinitrobenzenesulfonic acid or with antibiotics

To induce inflammation, zebrafish larvae were either untreated or treated with 2,4,6-Trinitrobenzenesulfonic acid (TNBS; Sigma Aldrich P2297) from day 3 post-fertilization until 120 hpf. TNBS was added in a 1:1000 dilution in E3 water (final concentration: 50 μg/mL) and replaced every 24 hours. To deplete the bacterial content, zebrafish larvae were treated with an antibiotic cocktail from day 3 post-fertilization until 120 hpf (Bates et al., 2006). The antibiotic cocktail consists of Ampicillin (100 μg/ml) and Kanamycin (5 μg/ml) that was added to E3 water and replaced every 24 hours.

Treatment of mice with antibiotics

WT mice were treated with antibiotic cocktail for 10 consecutive days by oral gavage. The antibiotic cocktail contains Ampicillin (1mg/ml), Kanamycin (1mg/ml), Gentamicin (1mg/ml), Metronidazole (1mg/ml), Neomycin (1mg/ml), and Vancomycin (0.5mg/ml).

Preparation of sense and antisense Digoxigenin (DIG)-labeled RNA probes for detection of Gpr35b in zebrafish

DNA plasmid containing *Gpr35b* cDNA (5 μg) was linearized in a 2 h digestion, using SacI and EcoRI to generate the sense and antisense probe template, respectively. The linearized plasmid was purified by phenol: chloroform extraction method followed by ethanol

precipitation. Following successful production of template, the *in vitro* synthesis of the sense and antisense DIG-Labeled RNA probes were made in a 2 hours incubation at 37°C with the following transcription mix (20 μL): DNA template (1-2 μg), DIG-RNA labeling mix, protector RNase Inhibitor, transcription buffer and RNA Polymerase T7 and T3, respectively. Following the incubation, DNA template was digested by adding DNase I for 30 min at 37°C and was stopped by adding 2 μL of 0.2 M EDTA. DIG-Labeled RNA Probes were precipitated by LiCl method and resuspended in 30 μL Probe solution (19 μL sterilized water, 10 μL RNAlater and 1 μL 0.5M EDTA).

In situ hybridization for gpr35b detection in zebrafish

In situ hybridization (ISH) was performed in whole zebrafish larvae from the developmental stages 72 hpf, 96 hpf and 120 hpf. Those larvae were fixed by 4% paraformaldehyde (PFA) in PBS at 4°C overnight followed 3 PBS washes. Progressive dehydration by washing for 5 min in 25%, 50% and 75% methanol in PBS and final 5- and 15-min wash in 100% methanol were performed. In some cases, the depigmentation method was required due to their developmental stage. In this case, larvae were treated with 3% H_2O_2/0.5% KOH at RT until pigmentation has completely disappeared and then progressive dehydration was performed as described above. Larvae were placed at −20°C for at least 2 h. After incubation, larvae were rehydrated, washed 4 times with PBST (0.1% Tween-20 in PBS) followed by proteinase K (10 μg/mL) treatment at RT for a time defined by the developmental state such is indicated coming up next: 72 hpf – 20 min; 96 hpf – 30 min; and 120 hpf – 40 min. Proteinase K digestion was stopped by incubating the larvae for 20 min in 4% PFA. Larvae were washed with PBST and prehybridized with 700 μL hybridization mix (HM) solution (50% deionized formamide (Millipore); 0.1% Tween-20 (Sigma); 5X saline sodium citrate solution (Merck); 50mg/ML of heparin (Sigma); 500 mg/mL RNase-free tRNA (Sigma)) for 5 h at 70°C. HM solution was replaced by 200 μL of HM containing 50 ng of antisense/sense DIG-labeled RNA probe and incubated overnight at 70°C. Then the larvae went through several washing steps with SSC and PBST solution followed by incubation with blocking buffer for 4h at RT. Afterward, larvae were incubated with anti-DIG-AP antibody solution overnight at 4°C. Subsequently, they were washed 6 times for 15 min with gentle agitation on a horizontal shaker, incubated with alkaline Tris buffer for 5 min at RT with gentle agitation, and stained in the dark using 700 μL staining solution. When the color was developed, the reaction was stopped by adding stop solution (1mM EDTA and 0.1% Tween-20 in PBS pH 5.5). Finally, larvae were transferred to a tube containing 100% glycerol and kept in this solution at least 24 h before mounting them.

Challenging of mice with *E. coli*-CFP

We used *E. coli* DH10B pCFP-OVA described previously (Rossini et al., 2014). Gpr35-tdTomato x Cx3cr1-GFP mice were gavaged every other day for 21 days with $1x10^8$ CFUs of CFP-OVA$^+$ *E. coli* and sacrificed for further analysis.

Exposure of zebrafish with Vibrio anguillarum

V. anguillarum strain 1669 (Hernández et al., 2018) was grown in tryptic soy broth medium to OD_{600} (optical density at 600 nm) 1.5. Bacterial pellet (9 mL of full-grown culture) was resuspended in NaCl (9 g/L), 0.35% formaldehyde, and incubated overnight at 20°C. The suspension was washed four times in NaCl(9 g/L) and resuspended in 800 mL of the same isotonic solution. *V. anguillarum* extract was mixed in a 1:1 ratio with phenol red (Sigma Aldrich P0290). One μL of this mixture was diluted with 2 μL PBS from which 2 nL were used to be injected in the swim bladder and intestinal region of 110 hpf zebrafish larvae. Larvae were anesthetized using 0.0016% Tricaine MS0222 (Sigma-Aldrich E10521). Larvae were then monitored for recovery and analyzed 6 h post-injection.

LPA injection in zebrafish

LPA (10 μM) or equal volume of DMSO were mixed with FITC-Dextran (500 μg/ml) in PBS. For the challenge, 2 nL were injected in the otic vesicle of 110 hpf larvae anesthetized with 0.0016% Tricaine MS-222. Larvae were then monitored for recovery and macrophage recruitment was analyzed 6 h after the injection.

Stimulation of zebrafish larvae with LPA

WT and *gpr35b*^{uu1892} zebrafish larvae were either left unstimulated or stimulated with 10 μM LPA (Sigma L7260) in water from 96 hpf until 120 hpf. After the incubation, zebrafish larvae were lysed, RNA extracted, and cytokine production was evaluated by qPCR using primers listed in Table S1.

Cell Isolation from the small and large intestinal lamina propria, mesenteric lymph nodes and spleen

Colonic lamina propria cells were isolated as described previously (Radulovic et al., 2019; Steinert et al., 2017). Briefly, extracted colon or small intestine segments were opened longitudinally and washed with PBS (Sigma-Aldrich). IECs were dissociated using 5 mM EDTA at 37°C in a shaking water bath at 200 rpm for 10 minutes. The dissociation step was repeated in fresh EDTA solutions for 2 additional times. The tissue was vortexed for 30 s before and after each incubation and IECs were collected for further processing, if necessary. After removing IECs, the tissue was immersed in PBS to wash the EDTA away and cut into small pieces for digestion. The tissue was digested in Roswell Park Memorial Institute (RPMI) 1640 (Sigma-Aldrich) containing 0.5 mg/ml Collagenase type VIII (Sigma-Aldrich) and 10 U/mL DNase (Roche) for 15-20 min at 37°C in shaking water bath with 30 s vortexing each 5 min. Digested tissue was passed through a 70 μm cell strainer and the single cell suspension was pelleted for further analysis.

Spleen and MLN cells were isolated by mashing the tissue with a syringe plunger on a 70 μm cell strainer. Spleen red blood cells (RBCs) were lysed using ammonium-chloride-potassium buffer (150 mM NH_4Cl, 10 mM $KHCO_3$, 0.1 mM 0.5 M EDTA). The remaining cells were pelleted for further use.

Antibodies, cell staining and flow cytometry

Up to $5x10^6$ isolated cells were incubated for 30 min at 4°C with anti-CD16/CD32 (Fc receptor) clone 93 (Invitrogen) to block non-specific binding and with fixable viability dye eFluor455UV (eBioscience) for live/dead cell exclusion. Cells were washed in PBS containing 2% Fecal Bovine Serum (FBS), 0.1% sodium azide, and 10 mM EDTA (FACS buffer) and stained for surface antigens for 20 min at 4°C. For intracellular staining, cells were further fixed and permeabilized in Cytofix/Cytoperm solution according to the manufacturer's instructions (BD Biosciences) followed by incubation with antibodies against intracellular antigens for 20 min at 4°C. Cells were then resuspended in FACS buffer and flow cytometric analysis was performed on a Fortessa flow cytometer (BD Biosciences). Data were analyzed using FlowJo software version 10.0.7r2 (TreeStar). In all experiments, doublet discrimination was done on forward scatter (FSC-H) versus FSC-A plot. Mononuclear phagocyte staining was done using antibodies eVolve655-conjugated anti-CD45 clone 30-F11 (eBioscience), biotin-labeled anti- CD3 clone 145-2C11, anti- CD19 clone 6D5 and anti-NK.1.1 clone PK136, AF700-conjugated anti- I-A/I-E (MHCII) clone M5/114.15.2, PE/Cy7-conjugated anti- CD64 clone X54-5/7.1, APC/Cy7-conjugated anti-CD11c clone N418, FITC-conjugated anti- CD11b clone M1/70, PerCP/Cy5.5- conjugated anti-Ly6C clone HK1.4, and APC-conjugated anti- Ly6G clone 1A8 (all BioLegend). For lineage exclusion, $CD3^+$, $CD19^+$ and $NK1.1^+$ cells were gated out. For lymphocyte staining, antibodies for APC/Cy7-conjugated anti-CD45 clone 30-F11, AF700- conjugated anti-CD3 clone 17A2, BV785-conjugated anti-CD19 clone 6D5, BV510-conjugated anti-CD4 clone RM4-5 and PerCP-conjugated anti-CD8a clone 53-6.7 or biotin-labeled anti-CD8 clone 53-6.7 (all BioLegend) were used. For innate lymphoid cell panel, antibodies APC/Cy7- conjugated anti-CD90.2 clone 30-H12 (BioLegend), APC-conjugated anti-GATA3 clone 16E10A23 (BioLegend), PerCP/Cy5.5-conjugated anti-RORγT clone Q31-378 (BD Biosciences), PE/Cy7-conjugated anti-T-bet clone 4B10 (BioLegend) and FITC-conjugated anti-Eomes clone WD1928 (Invitrogen) were included whereas biotin-conjugated antibodies anti-CD3 145-2C11, anti-CD8a 53-6.7, anti-CD19 6D5, anti-CD11c N418 (all BioLegend), anti-B220 RA3-6B2 (BD Biosciences), anti-Gr-1 RB6-8C5, anti-TCRβ H57-597, anti-TCRγδ GL3 and anti-Ter119 TER-119 (all BioLegend) were used for lineage exclusion. eFluor450 conjugated Streptavidin (eBioscience) was used for all biotin-labeled antibodies.

RNA extraction and quantitative PCR

RNA was extracted from cells, mouse or zebrafish tissues, whole zebrafish larvae or human biopsies using TRI Reagent (Zymo Research) or TRIzol (Invitrogen) according to the manufacturer's instructions. For DSS-treated mouse colonic tissue, Direct-zol RNA MiniPrep kit (Zymo Research) was used to remove the DSS residues. RNA samples were treated with TURBO DNase (Invitrogen) and reverse transcribed using High Capacity cDNA Reverse Transcription (Applied Biosystems) or iScript cDNA synthesis (Bio-Rad) kits by following manufacturer's instructions. Quantitative PCR was performed using primers listed in Table S1 and QuantiNova SYBR Green PCR (QIAGEN) or iTaq Universal SYBR® Green Supermix (Bio-Rad) kits. Samples were run on an ABI ViiA 7 cycler or a CFX384 Touch Real-Time PCR. Ct values were normalized to that of *efa1*, *Hrpt*, *Gapdh* or *Actb,* and relative expression was calculated by the formula $2^(-\Delta Ct)$. Used primers are listed in Table S1.

Immunofluorescence staining

Human biopsies were provided by the Basel IBD cohort in cryoblocks. Mouse tissues were fixed with 4% PFA and left in 30% sucrose overnight for cryo-embedding or dehydrated in ethanol solutions for paraffin embedding. All tissues were sectioned at 6 μm and fixed with 4% PFA. Blocking and permeabilizing were done using PBS containing 0.4% Triton X-100 for cryosections or 0.1% Tween20 for paraffin sections and 5% goat serum (all Sigma-Aldrich). Tissue sections were stained with rabbit polyclonal anti-human/mouse GPR35 primary antibody and goat anti-rabbit IgG secondary antibody. For all samples, NucBlue™ Live Cell Stain (Thermo Fisher) was used for nuclear staining and samples were imaged using a Nikon A1R confocal microscope.

Autotaxin staining

Mouse tissues were fixed with 4% PFA and dehydrated in ethanol solutions for paraffin embedding. All tissues were sectioned between 5-6 μm. Endogenous peroxidase activity was blocked with 3% H_2O_2 solution in methanol and antigen retrieval to unmask the antigenic epitope was performed with EDTA buffer (1mM EDTA, pH 8.0). Blocking was done using BLOXALL Blocking Solution (Vector Laboratories SP-6000). Tissue sections were stained with mouse monoclonal anti-ENPP2 (autotaxin) Mouse/Human primary antibody (Abcam ab77104) and goat anti-rabbit IgG secondary antibody. All samples were additionally stained with H&E as described previously.

Ex vivo imaging of colonic tissues

Extracted colon was washed with PBS, opened longitudinally and placed on a slide. A drop of PBS was added to prevent the tissue from drying and tissue was covered with a coverslip. Tissues were imaged on a Nikon A1R confocal microscope.

RNA sequencing

For colonic macrophages, RNA was isolated from sorted GPR35^{+} and GPR35^{-} colonic macrophages from 1 or 2 *Gpr35*-tdTomato mice. RNA quality control was performed with an Agilent 2100 Bioanalyzer and the concentration was measured by using the Quanti-iT RiboGreen RNA assay Kit (Life Technologies). cDNA was prepared using SMART-Seq v4 Ultra Low Input RNA Kit (Tamara). Sequencing libraries were prepared using Nextera XT DNA Library Preparation Kit (Illumina). Indexed cDNA libraries were pooled in equal amounts and sequenced SR81 with an Illumina NextSeq 500 Sequencing system.

For BMDMs, RNA was isolated following lysing of cells derived from WT or *Gpr35*$^{-/-}$ mice. RNA were quality-checked on the TapeStation instrument (Agilent Technologies) using the RNA ScreenTape (Agilent Technologies) and quantified by Fluorometry using the QuantiFluor RNA System (Promega). Library preparation was performed, starting from 200ng total RNA, using the TruSeq Stranded mRNA Library Kit (Illumina) and the TruSeq RNA UD Indexes (Illumina). Samples were pooled to equal molarity. Libraries were sequenced Paired-End 51 bases using the NovaSeq 6000 instrument (Illumina) Primary data analysis was performed with the Illumina RTA version 3.4.4.

Reads were aligned to the mouse genome (UCSC version mm10) with STAR (version 2.5.2a) using the multi-map settings '-outFilterMultimapNmax 10–outSAMmultNmax 1' (Dobin et al., 2013). Read and alignment quality was evaluated using the qQCReport function of the R/Bioconductor package QuasR (R version 3.4.2, Bioconductor version 3.6) (Gaidatzis et al., 2015). Assignment of reads to genes employed the UCSC refGene annotation (downloaded 2015-Dec-18). QuasR function qCount function was used to count the number of read (5′ends) overlapping with the exons of each gene assuming an exon union model. In case of unstranded SMART-Seq 4 data, reads mapping to both strand where counted, while the True-Seq data only considered reads on the opposite strand of the feature. Differential gene expression analysis was performed using the R/Bioconductor package edgeR (McCarthy et al., 2012). After filtering genes with logCPM > 1 in at least 1 sample, two models were used for testing different aspects of genotype and treatment effects. A nested design analysis was performed contrasting treatment groups within each genotype. For the comparison across genotypes a non-nested model with crossed genotype-treatment groups was chosen. Both models employed different gene dispersion estimates. The glmQLFit and glmQLFTest functions of edgeR were used to test the respective model contrasts. Resulting P values were false discovery rate adjusted. RNA-seq data shown in Figure 4B was obtained from a dataset published elsewhere (Czarnewski et al., 2019).

3′-5′-Cyclic adenosine monophosphate (cAMP) assay

To screen potential GPR35 ligands, the cAMP Hunter^{TM} eXpress assay platform (Eurofins) was used according to the manufacturer's directions. Briefly, GPR35-transfected CHO-K1 cells were thawed and 3x10^{5} cells were seeded on a 96-well plate followed by overnight incubation at 37°C, 5% CO_2. Cells were treated at 37°C for 30 minutes with 15 μm Forskolin and 1:3 serial dilutions of potential ligands with the following starting concentrations: 10 μM recombinant human CXCL17 (R&D Systems), 10 μM lysophosphatidic acid (LPA) or 10 mM kynurenic acid (KYNA) (both Sigma-Aldrich). Zaprinast (Sigma-Aldrich) was used as a positive control. cAMP levels were measured by enzyme-fragment complementation (EFC) technology, where two fragments of β- galactosidase were used. In the presence of cAMP, cAMP labeled with one part of the enzyme is outcompeted to bind to anti-cAMP antibody and therefore is free to complement the enzyme complex and cleave the substrate to produce a luminescent signal. The signal was then measured by Synergy H1 Microplate Reader (Biotek).

Mouse bone marrow-derived macrophages

Femur and tibias from WT or *Gpr35*-deficient mice were cut at both ends and bone marrow was flushed out with PBS with the help of a syringe with a 25-gauge needle. The cells were collected and cultured in RPMI 1640 containing 10% FBS, 0.05 mM 2-ME, 100 U/mL penicillin and 100 μg/mL streptomycin supplemented with 20 ng/mL M-CSF (BioLegend) at a density of 2x10^{5} cells/mL. Cells were incubated at 37°C, 5% CO_2, and the medium was exchanged on days 3 and 5 of the culture. On day 7, the BMDMs were stimulated with 10 μM LPA or 10 ng/mL LPS for 1 hour, 4 hours or 24 hours for western blot, RNA extraction or cytokine detection by LEGENDplex^{TM}.

Cytokine detection by LEGENDplex^{TM} bead-based immunoassay

Concentrations of TNF, IL-1α, IL-1β and IL-23 were measured in the supernatants of BMDMs that were left untreated or were treated with LPA or LPS for 24 hours. For detection, bead-based immunoassay LEGENDplex^{TM} (Biolegend) was used following the manufacturer's instructions.

Western blot analysis of LPA- or LPS- treated BMDMs

Following treatment, the cells were lysed with ice-cold RIPA buffer containing sodium orthovanadate, PMSF, protease inhibitor cocktail (Santa Cruz) according to the manufacturer's recommendations. Protein concentrations were quantified using the BCA method. 10 μg of each protein sample was transferred onto a nitrocellulose membrane by electrophoretic separation. The membranes were blocked using 5% dry milk in Tris Buffered Saline + Tween20 (TBS-T) buffer. The following primary antibodies were used: phospho-NF-κB (p65), NF-κB, phospho- ERK1/2, ERK1/2, phospho- STAT3, STAT3 (all from Cell Signaling Technology) and β-actin (BD Biosciences) at 1:1000 or 1:2000 dilution for western blotting. The horseradish peroxidase-conjugated secondary antibodies anti-rabbit

IgG (H+L) and anti-mouse IgG (H+L) (both Jackson ImmunoResearch) were used at 1:30000 dilution prior to detection with SuperSignalTM West Femto or SuperSignal West Pico PLUS (both Thermo Fisher) chemiluminescent detection kits.

Transwell migration assay for quantification of BMDM migration

$5x10^5$ BMDMs were seeded on inserts with a 5 μm pore size (Corning). RPMI 1640 containing 2% FBS with 10 μM LPA was placed in the outer chamber. The cells were allowed to migrate for 18 hours. Migrated cells and the cells in the upper chamber were collected and resuspended in 200 μL of FACS buffer. 70 μL of each sample was acquired using BD Accuri^{TM} C6 flow cytometer (BD Biosciences) and the percentage of migrated cells was calculated.

Enzyme-linked immunosorbent assays (ELISA) for corticosterone and LPA detection

Corticosterone concentrations were determined in mouse colonic explants, which had been incubated for 24 hours in 24-well plates in 500 μL of DMEM containing 2% FBS and 100 U/mL penicillin and 0.1 mg/mL streptomycin. Corticosterone or LPA levels were determined using the Corticosterone Competitive ELISA kit (Invitrogen) or General LPA ELISA kit (MyBioSource) and normalized to the weights of colon pieces measured before the assay.

Characterization of anti-TNF blocker responses in GPR35^{T108M} IBD patients

Baseline characteristics for the IBD patients enrolled in the Swiss IBD Cohort Study are summarized in Table S4 (SwissIBD cohort project 2017-13). For identification of GPR35^{T108M} variant, SNPs were genotyped by Sequenom, Hamburg, Germany, using genomic DNA samples at a concentration of 5-10 ng/μl of genomic DNA. Genotyping was done by the mass spectrometric analysis of the primer extension products. GPR35^{T108M} IBD patients were analyzed for breakthrough/loss of response, primary non-response (never effective) and side effects/intolerance in response to TNF blockers.

QUANTIFICATION AND STATISTICAL ANALYSIS

Data are presented as dot plots of individual values with medians. GraphPad Prism software was used to graph the data and calculate statistical significance. P values were calculated using either unpaired t test, Mann-Whitney U or two-way ANOVA tests depending on the experimental setting. Data were further analyzed by Grubbs' test to identify the outliers. For all tests p values were indicated as followed: *$p < 0.05$, **$p < 0.01$, ***$p < 0.001$

Cell Reports, Volume *32*

Supplemental Information

Lysophosphatidic Acid-Mediated GPR35 Signaling in CX3CR1^{+} Macrophages Regulates Intestinal Homeostasis

Berna Kaya, Cristian Doñas, Philipp Wuggenig, Oscar E. Diaz, Rodrigo A. Morales, Hassan Melhem, Swiss IBD. Cohort Investigators, Pedro P. Hernández, Tanay Kaymak, Srustidhar Das, Petr Hruz, Yannick Franc, Florian Geier, C. Korcan Ayata, Eduardo J. Villablanca, and Jan Hendrik Niess


A
hsGPR35 -----MNGTYNTCGSSDLTWPPAIKLGFYAYLGVLLVLGLLLNSLALWVFCCR-MQQWTE
mmGPR35 --------MNSTTCNSTLTWPASVNNFFIIYSALLLVLGLLLNSVALWVFCYR-MHQWTE
Gpr35a MSSTRAFEQGFAMSNCTLNLNDSILTLQKVTSIPMFVLGMLGNIYVLVKFCWRPKTQWTY
Gpr35b -----MALVDFNCSAVRSQTDAAISLFERVAYPPVFIVGLSFNITALYLFCRI--KRWTD
hsGPR35 TRIYMTNLAVADLCLLCTLPFVLHSLRDTS---DTPLCQLSQGIYLTNRYMSISLVTAIA
mmGPR35 TRIYMTNLAVADLCLLCSLPFVLYSLKYSSS--DTPVCQLSQGIYLANRYMSISLVTAIA
Gpr35a MNIYISNMVAADCALLIFLPVKIHYYNRELAGGLQKLCNFVLSLYYINMYVSIFTITAIS
Gpr35b THIYMLNLLVADLLAIVFLPFRILEAFCQIKP--TILCTFLLCTQYSNMYCSMFTITAIS
hsGPR35 VDRYVAVRHPLRARGLRSPR--QAAAVCAVLWVLVIGSLVARWLLGIQEG---GFCFR--
mmGPR35 VDRYVAVRHPLRARELRSPR--QAAAVCVALWVIVVTSLVVRWRLGMQEG---GFCFSS-
Gpr35a VVRYVAIKYPMKAREIFSCR--SALVVCAVIWVTICSISPVYFVTDSSNDKTMCFQRVK-
Gpr35b VHRFISVRFPFFLTKSLVSKSKAIAITKCIVIWIIIAVICASNYRDLMPDNLDGCYDLNLT
hsGPR35 STRHNFNSMAFPLLGFYLPLAVVVFCSLKVVTALAQRPPTDVGQ-AEATRKAARMVWANL
mmGPR35 QTRRNFSTTAFSLLGFYLPLAIVVFCSLQVVTVLSRRPAADVGQ-AEATQKATHMVWANL
Gpr35a QTLSLHFILLLIIVGFVLPFIIMLYCSARVIHTLR--KQLDVGS-RSEKLQCMFIIIANL
Gpr35b FTFIVCFTPVHIGLLLQYLSDEN----------GKNFIHVFLDVAEWIATTNCCLDAIG
hsGPR35 YYYMAKEFQEASALAVAPSAKAHKSQDSLCVTLA
mmGPR35 YYYMAREFQEASKPATS-SNTPHKSQDSQILSLT
Gpr35a YFFATKTSWNMCCTGQAKNEKSRYNTVSDSDGKS
Gpr35b YYFLLKRIHKGENSFN----------
Sequence 1: hGPR35 309 aa
Sequence 2: mmGPR35 307 aa
Sequence 3: Gpr35a 328 aa
Sequence 4: Gpr35b 296 aa
Sequences (1:2) Aligned. Score: 69.0554
Sequences (1:3) Aligned. Score: 25.5663
Sequences (1:4) Aligned. Score: 23.9865
Sequences (2:3) Aligned. Score: 24.43
Sequences (2:4) Aligned. Score: 24.3243
Sequences (3:4) Aligned. Score: 25.6757

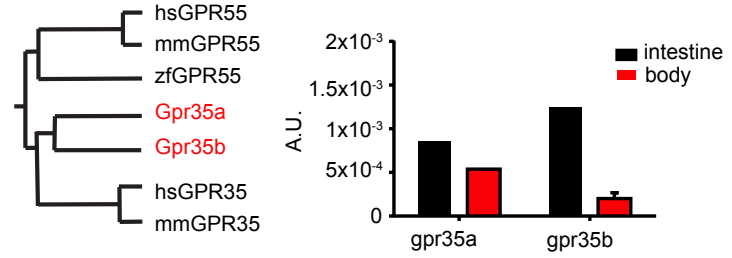
B
hsGPR55
mmGPR55
zfGPR55
Gpr35a
Gpr35b
hsGPR35
mmGPR35
C
2x10-3
1.5x10-3
1x10-3
5x10-4
0
A.U.
intestine
body
gpr35a
gpr35b

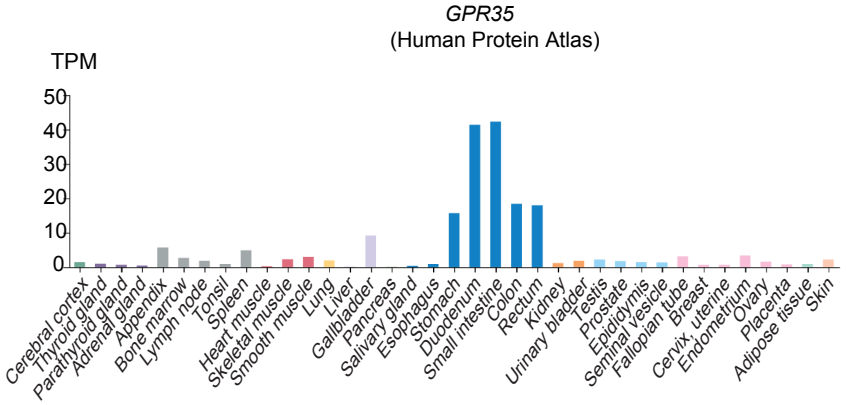
D
GPR35
(Human Protein Atlas)
TPM
50
40
30
20
10
0
Cerebral cortex
Thyroid gland
Parathyroid gland
Adrenal gland
Appendix
Bone marrow
Lymph node
Tonsil
Spleen
Heart muscle
Skeletal muscle
Smooth muscle
Lung
Liver
Gallbladder
Pancreas
Salivary gland
Esophagus
Stomach
Duodenum
Small intestine
Colon
Rectum
Kidney
Urinary bladder
Testis
Prostate
Epididymis
Seminal vesicle
Fallopian tube
Breast
Cervix, uterine
Endometrium
Ovary
Placenta
Adipose tissue
Skin

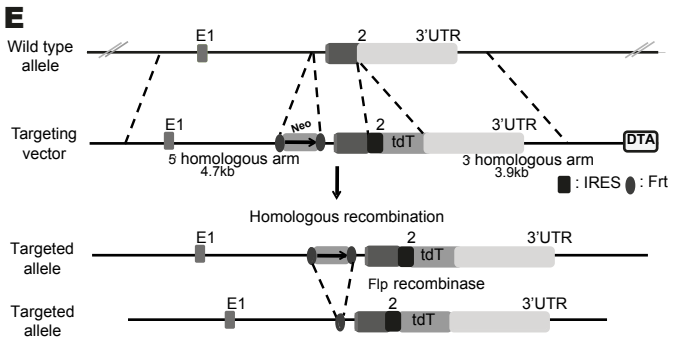
E
Wild type allele
E1
2
3'UTR
Targeting vector
E1
neo
2
tdT
3'UTR
DTA
5 homologous arm
4.7kb
3 homologous arm
3.9kb
: IRES : Frt
Homologous recombination
Targeted allele
E1
2
tdT
3'UTR
Flp recombinase
Targeted allele
E1
2
tdT
3'UTR

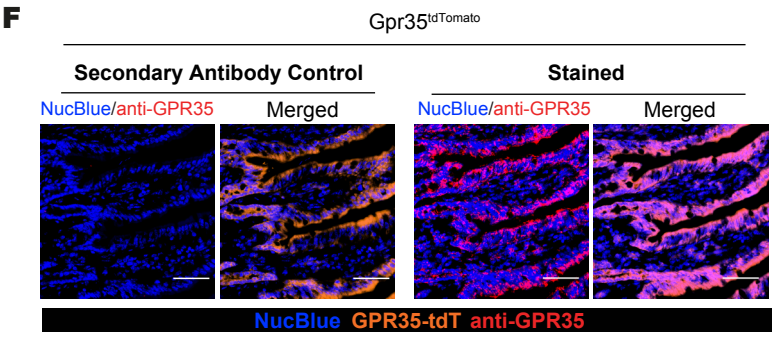
F
Gpr35tdTomato
Secondary Antibody Control
Stained
NucBlue/anti-GPR35
Merged
NucBlue/anti-GPR35
Merged
NucBlue GPR35-tdT anti-GPR35

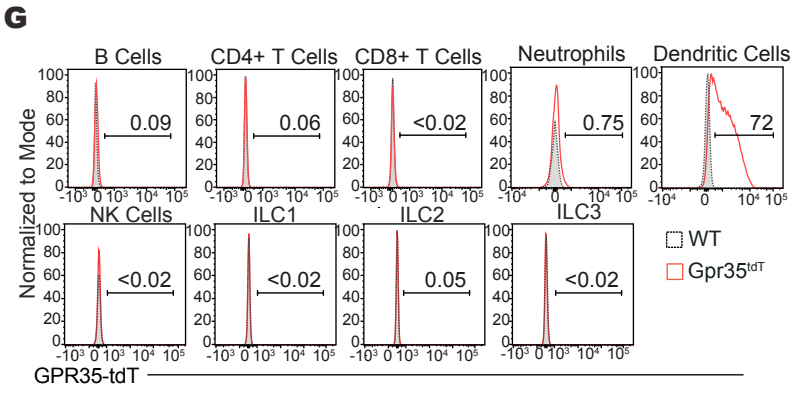
G
B Cells
CD4+ T Cells
CD8+ T Cells
Neutrophils
Dendritic Cells
0.09
0.06
<0.02
0.75
72
NK Cells
ILC1
ILC2
ILC3
<0.02
<0.02
0.05
<0.02
Normalized to Mode
WT
Gpr35tdT
GPR35-tdT

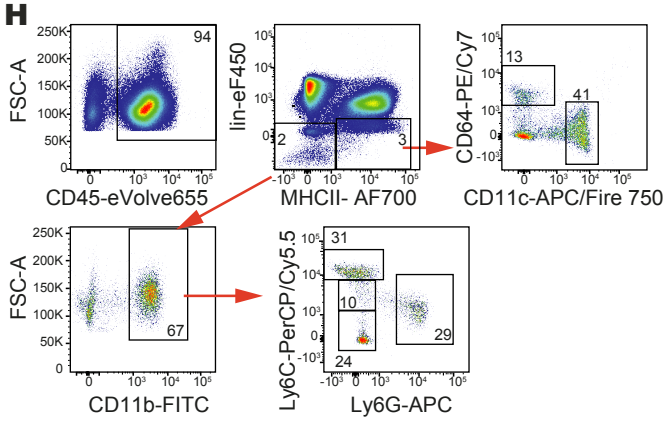
H
FSC-A
94
CD45-eVolve655
lin-eF450
2
3
MHCII- AF700
CD64-PE/Cy7
13
41
CD11c-APC/Fire 750
FSC-A
67
CD11b-FITC
Ly6C-PerCP/Cy5.5
31
10
29
24
Ly6G-APC

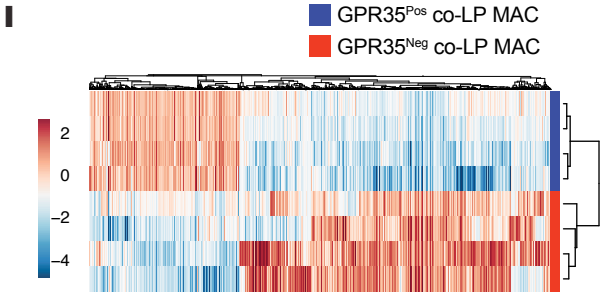
I
GPR35Pos co-LP MAC
GPR35Neg co-LP MAC
2
0
−2
−4

Figure S1. Zebrafish, mouse, and human GPR35 expression, Related to Figure 1

(A) ClustalW alignment of mouse and human GPR35 with Gpr35a and Gpr35b paralogs identified in zebrafish (red). Alignment scores per pair of sequences were calculated by ClustalW.

(B) Phylogenetic tree including protein sequences from human, mouse, and zebrafish *GPR35* and *GPR55* orthologs. Analysis was performed by ClustalW.

(C) *gpr35a* and *gpr35b* mRNA levels in the dissected intestine or rest of the body from WT zebrafish larvae. Target genes were normalized to *ef1a* housekeeping gene. One representative experiment is shown from two experiments.

(D) *GPR35* mRNA levels retrieved from the Human Protein Atlas (https://www.proteinatlas.org).

(E) Construct design of *Gpr35*-tdTomato reporter mice.

(F) Immunofluorescence staining of GPR35 and secondary antibody control in small intestine from *Gpr35*-tdTomato mice. Sections were stained for GPR35 (red) and NucBlue (blue) for nuclear staining. Scale bars, 50 μm.

(G) Percentage of *Gpr35*-tdTomato-positive B cells, $CD4^+$ T cells, $CD8^+$ T cells, neutrophils, dendritic cells, NK cells, ILC1 cells, ILC2 cells, and ILC3 cells in the colonic lamina propria of *Gpr35*-tdTomato reporter mice (red unfilled histograms) and WT mice (gray histograms) as the background control.

(H) Gating strategy for the analysis of colonic lamina propria monocytes and macrophages. Lin: lineage to exclude CD3, CD19, and $NK1.1^+$ cells.

(I) Unsupervised heatmap expression profile from RNA sequencing of *Gpr35*-tdTomato-positive (Pos) and negative (Neg) colonic lamina propria macrophages (co-LP MAC).

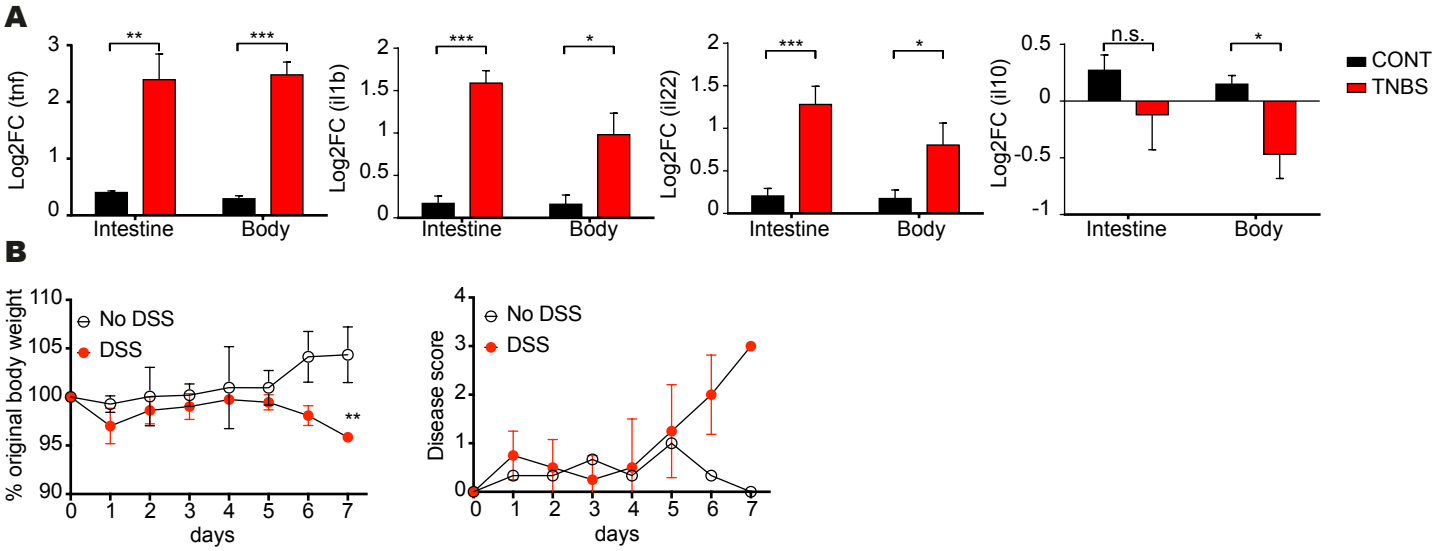

Figure S2. Intestinal inflammation in zebrafish and mice models, Related to Figure 2
(A) mRNA levels of cytokine genes *tnf, il1b, il22* and *il10* by qPCR in the intestine and rest body of control and TNBS-treated WT zebrafish normalized to ef1a housekeeping gene. Results are cumulative of three independent experiments with 50 larvae and are represented as mean ± SD.
(B) Body weight changes shown in percentage compared to original body weight of untreated or DSS-treated Gpr35tdT mice during 7 days (left panel). Disease activity scores of untreated or DSS-treated Gpr35tdT mice monitored daily during 7 days (right panel). Data are represented as mean ± SD for 3, 4 mice per group.
*p<0.05, **<p 0.01 by Mann Whitney.

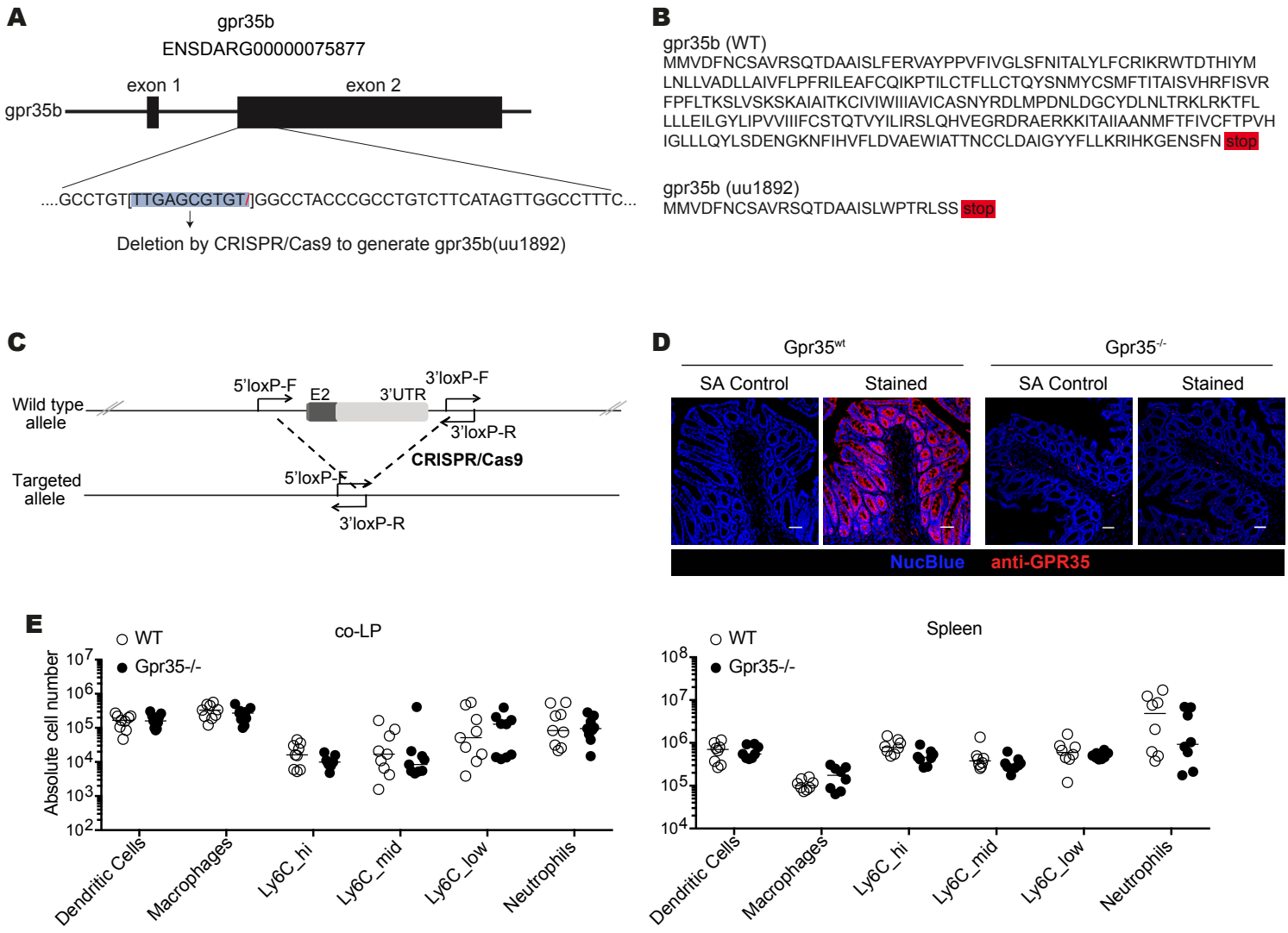

Figure S3. Construction of *gpr35b*^{uu1892} Zebrafish and *Gpr35*$^{-/-}$ Mice, Related to Figure 3

(A) Schematic representation of the *gpr35b* (ENSDARG00000075877) locus. The *gpr35b*^{uu1892} mutant line was generated by deletion of a 10-bp fragment within exon 2 (blue box).

(B) Schematic of the resulting Gpr35b proteins from WT or *gpr35b*^{uu19b2} mutant fish. Deletion results in a preliminary stop codon after the first 27 amino acids.

(C) Construct design for production of *Gpr35*$^{-/-}$ mice.

(D) Immunofluorescence staining of GPR35 in colon from *Gpr35*$^{-/-}$ (right) and WT mice (left). Sections were stained for GPR35 (red) and NucBlue (blue) for nuclear staining. Scale bars, 50 μm. Secondary antibody (SA).

(E) Number of dendritic cells, macrophages, Ly6Chi-mid or low monocytes and neutrophils in the colonic lamina propria (co-LP) or spleen of WT and Gpr35-/- mice calculated using flow cytometric analysis. Data are represented as individual values and median. Each dot represents one biological replicate.

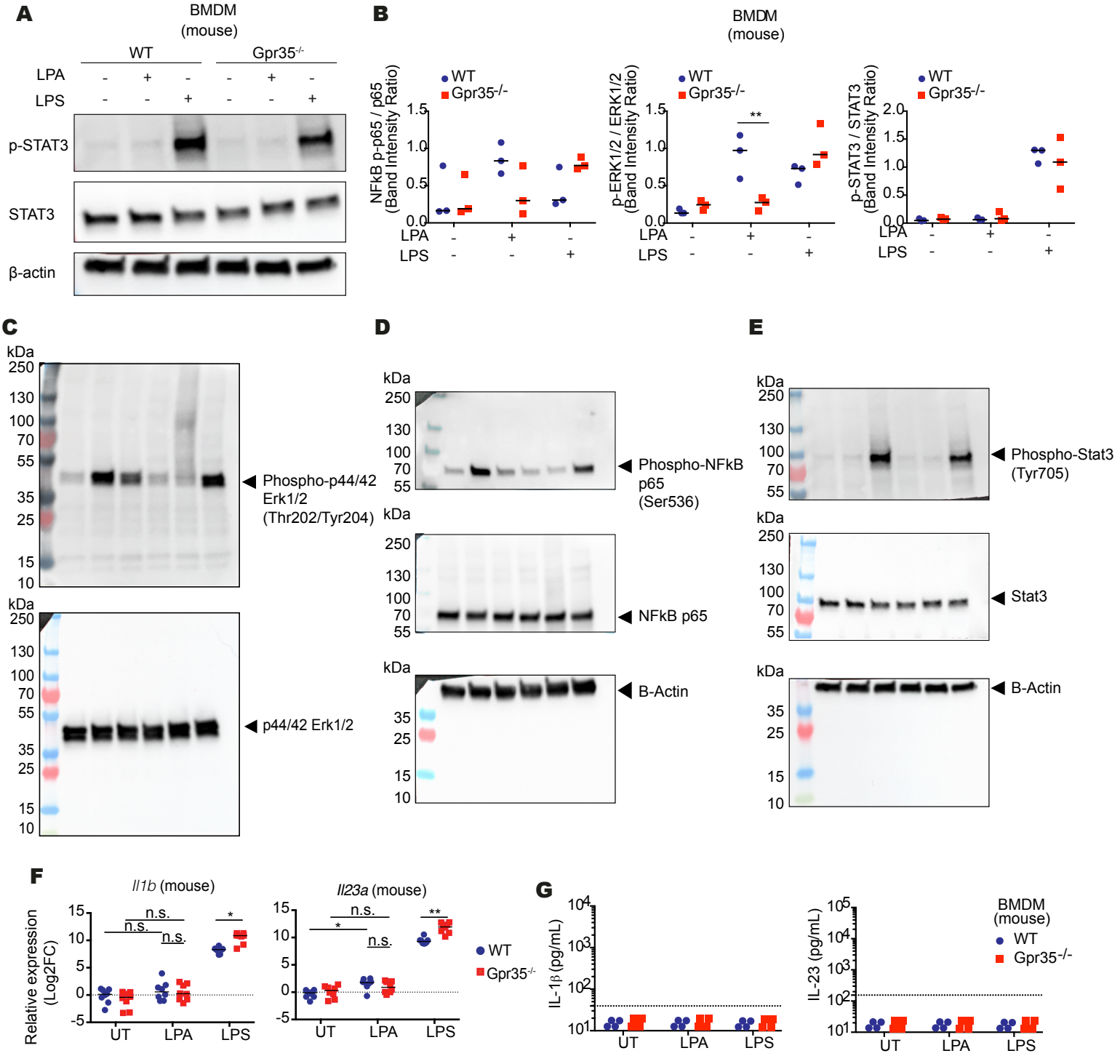

Figure S4. LPA signaling is mediated by GPR35 in mouse BMDMs, Related to Figure 3

(A) Western blot analysis of STAT3 phosphorylation in cell lysates from untreated, LPA- or LPS-treated BMDMs after 1 hour.

(B) Quantitative analysis of western blots (A) and (Figure 3D) shown as band intensity ratios between phosphorylated p65 (NF-kB), ERK1/2, STAT3 and the respective total proteins.

(C-E) Whole membrane images of western blots (A) and (Figure 3D)

(F) Fold changes in mRNA expressions of *Il1b* and *Il23a* by qRT-PCR normalized to *Actb* in WT or GPR35-deficient BMDMs that were untreated (UT) or treated with LPA or LPS.

(G) Concentrations of IL-1β and IL-23 in supernatants of untreated (UT), LPA- and LPS- treated BMDMs measured by LEGENDplex™ bead-based immunoassay.

Data are represented as dotplots and medians, each dot representing one biological replicate. *p<0.05, **p<0.01 by two-way ANOVA with Tukey's multiple comparisons test.

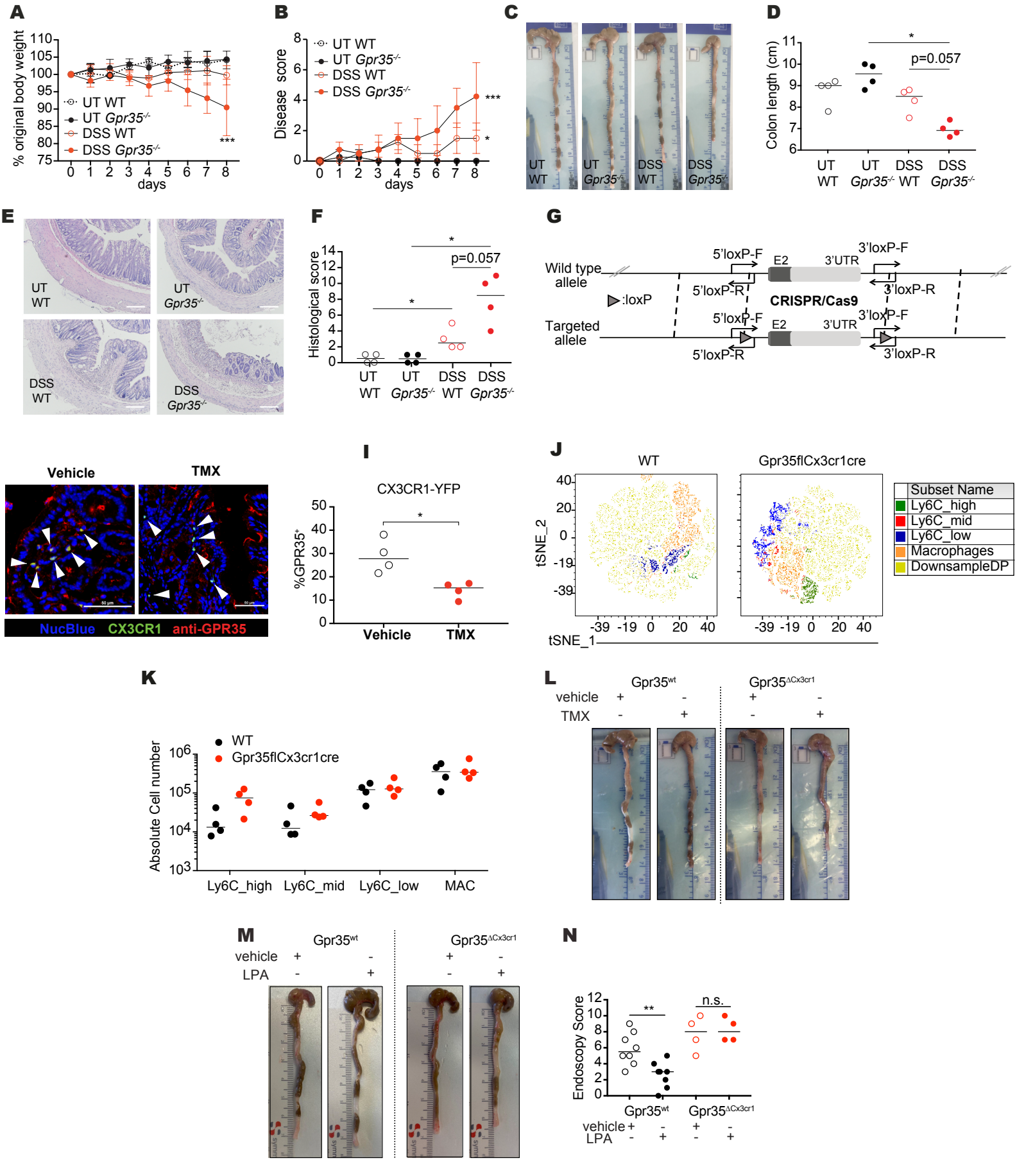
A
% original body weight
UT WT
UT Gpr35-/-
DSS WT
DSS Gpr35-/-
days
B
Disease score
C
UT WT
UT Gpr35-/-
DSS WT
DSS Gpr35-/-
D
Colon length (cm)
p=0.057
E
F
Histological score
p=0.057
G
Wild type allele
:loxP
Targeted allele
5'loxP-F
5'loxP-R
E2
3'UTR
3'loxP-F
3'loxP-R
CRISPR/Cas9
H
Vehicle
TMX
NucBlue CX3CR1 anti-GPR35
I
CX3CR1-YFP
%GPR35+
J
WT
Gpr35flCx3cr1cre
tSNE_1
tSNE_2
Subset Name
Ly6C_high
Ly6C_mid
Ly6C_low
Macrophages
DownsampleDP
K
Absolute Cell number
WT
Gpr35flCx3cr1cre
Ly6C_high
Ly6C_mid
Ly6C_low
MAC
L
Gpr35wt
Gpr35ΔCx3cr1
vehicle
TMX
M
Gpr35wt
Gpr35ΔCx3cr1
vehicle
LPA
N
Endoscopy Score
n.s.
Gpr35wt
Gpr35ΔCx3cr1
vehicle
LPA

Figure S5. Global and macrophage-specific GPR35-deficient Mice Show Exacerbated DSS Colitis, Related to Figure 5

(A) Percentages of body weight (normalized to initial weight) of untreated (UT) or DSS-treated WT or *Gpr35*$^{-/-}$ mice. Data are shown as mean ± SD for four mice per group.

(B) Disease activity scores assessed daily by monitoring UT or DSS-treated WT or *Gpr35*$^{-/-}$ mice. Data are shown as mean ± SD for fur mice per group.

(C) Representative images of colons from UT or DSS-treated WT or *Gpr35*$^{-/-}$ mice on day 8.

(D) Colon lengths measured from colon images as shown in (C) of UT or DSS-treated WT or *Gpr35*$^{-/-}$ mice on day 8.

(E) H&E staining of colon tissue sections from UT or DSS-treated WT or *Gpr35*$^{-/-}$ mice taken on day 8. Scale bars, 100 μm.

(F) Histology scores obtained from H&E staining of colons as shown in E.

(G) Construct design for production of *Gpr35*^{flox} mice.

(H) After mating of *Gpr35*^{flox} with *Cx3cr1*^{CreER} to obtain *Gpr35*$^{\Delta Cx3cr1}$mice, colon was taken from *Gpr35*$^{\Delta Cx3cr1}$mice injected i.p. with vehicle (left) or tamoxifen (right). Sections were stained for GPR35 (red) and NucBlue (blue) for nuclear staining. Arrowheads indicate CX3CR1-YFP^{+} macrophages. Scale bars, 50 μm.

(I) Percentages of GPR35^{+} cells among CX3CR1-YFP^{+} cells.

(J) t-SNE distribution of flow cytometry data for CD45^{+}Lin(CD19,CD3, NK1.1)$^{-}$ cells downsampled to 50000 events using colonic lamina propria of tamoxifen-injected WT and *Gpr35*$^{\Delta Cx3cr1}$ mice. Plots are representative for 1 mouse per group.

(K) Numbers of colonic lamina propria Ly6C$^{hi\text{-}mid\ or\ low}$ monocytes and macrophages (MAC) calculated from flow cytometric analysis (J).

(L) Representative colon images of vehicle- and tamoxifen (TMX)-treated WT and Gpr35$^{\Delta Cx3cr1}$ mice on day 7of DSS colitis.

(M) Representative colon images of WT and Gpr35$^{\Delta Cx3cr1}$ mice that received daily i.p. injections of vehicle or LPA taken on day 7 of DSS colitis.

(N) Endoscopy scores calculated from endoscopic imaging from (Figure 5J).

Data are represented as individual values, with each dot representing one mouse with medians (C-N). *p < 0.05, **p < 0.01, *** < p 0.001 by two-way ANOVA with Tukey's multiple comparisons test (A, B) or Mann-Whitney (D, F, I, N).

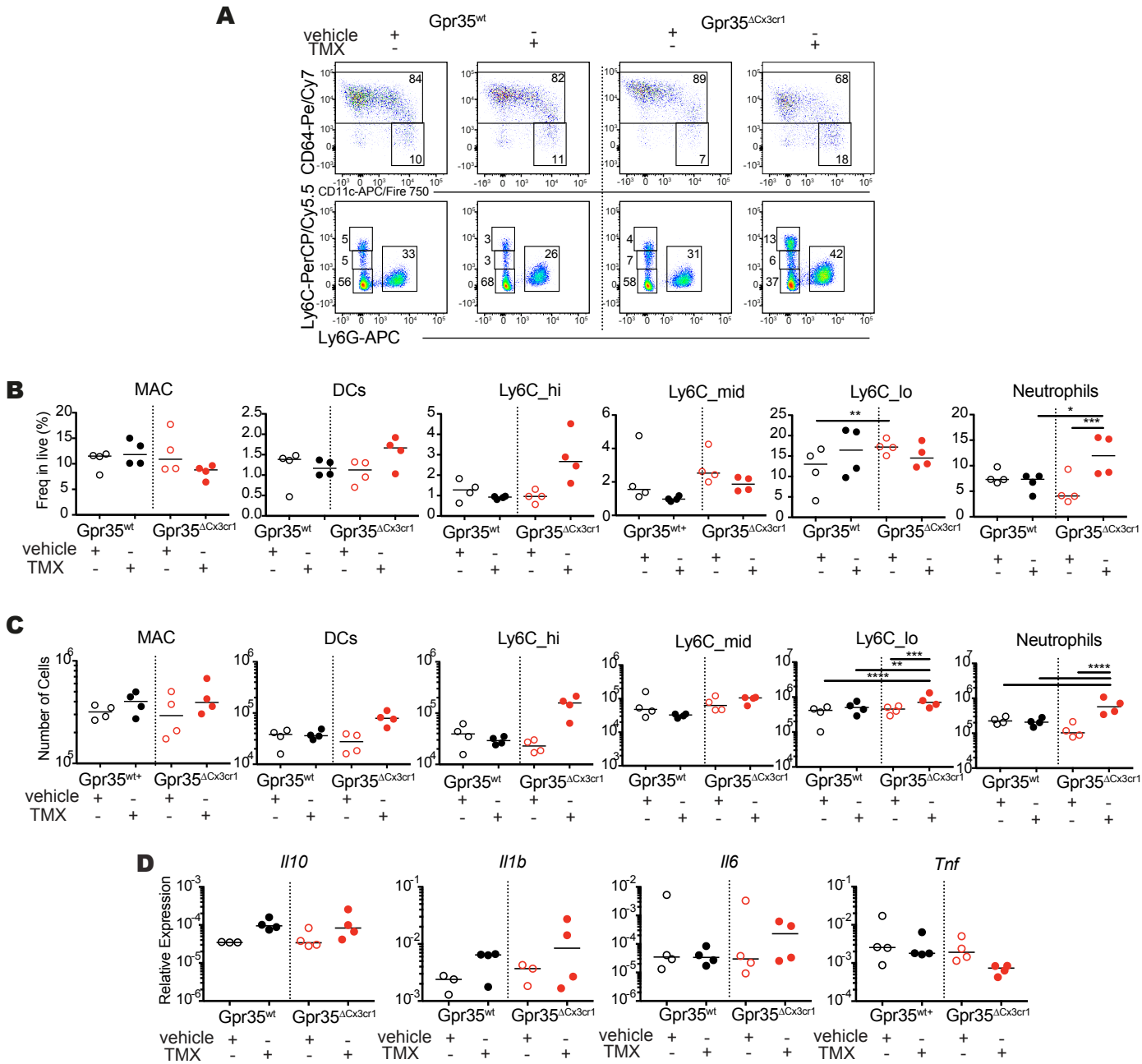

Figure S6. DSS-treated *Gpr35$^{\Delta Cx3cr1}$* mice Have Increased Neutrophil Numbers, Related to Figure 5

(A) Flow cytometric analysis of colonic lamina propria (co-LP) macrophages (MAC), dendritic cells (DCs), neutrophils and monocyte subsets (Ly6C^{high} to Ly6C^{low}) of vehicle-treated (corn oil) or tamoxifen (TMX)-treated WT or *Gpr35$^{\Delta Cx3cr1}$* mice on day 7 of DSS colitis. Quantification of flow cytometric data (B) for frequency (C) and number of macrophages, DCs, Ly6^{hi}, Ly6^{mid} or Ly6 ^{low} monocytes and neutrophils is shown below.

(D) mRNA expression levels of colonic *Il10*, *Il1b, Il6*, and *Tnf* relative to *Actb* by qRT-PCR of vehicle- or TMX-treated WT or *Gpr35$^{\Delta Cx3cr1}$* mice on day 7 of DSS colitis.

Data are presented as individual values with each dot representing one animal with medians. *p <0.05, **p <0.01, ***p <0.001 by Mann-Whitney.

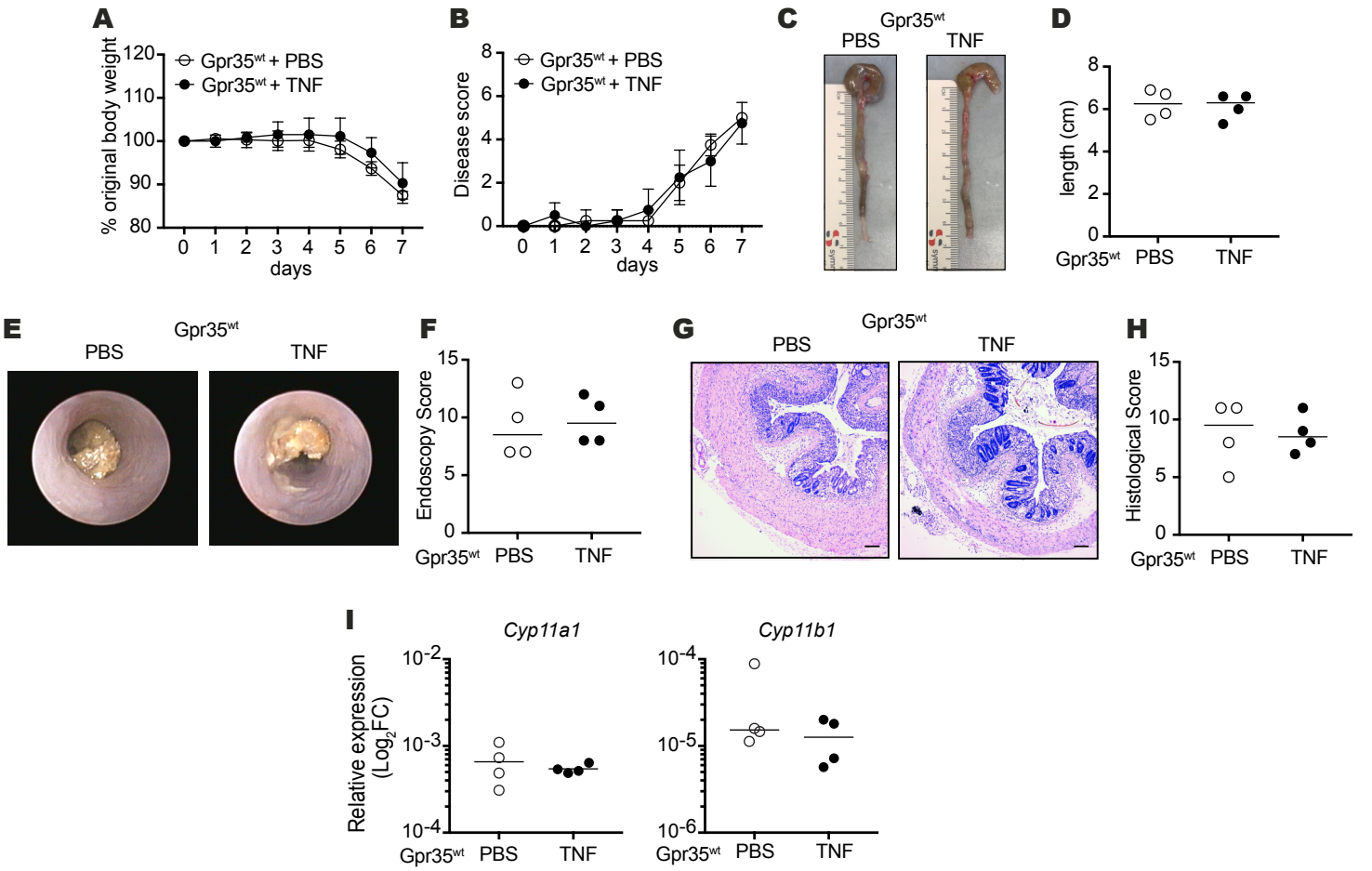

Figure S7. TNF does not have impact on DSS colitis severity in WT mice, Related to Figure 6
(A) Percentages of body weights compared to the original body weights of WT mice injected daily with PBS and TNF for 7 days of DSS colitis. Data are represented as mean ± SD for 4 mice per group.
(B) Colitis disease scores of WT animals administered with PBS and TNF assessed for 7 days of DSS colitis. Data are represented as mean ± SD for 4 mice per group.
(C) Representative colon images on day 7 of colitis from PBS- or TNF-treated WT mice.
(D) Colon lengths measured from (C)
(E) Representative endoscopic images of WT mice that received PBS or TNF injections daily taken on day 7 of DSS colitis.
(F) Endoscopy colitis scores determined from (E).
(G) H&E staining of colonic tissue from PBS- and TNF-treated WT mice on day 7 of DSS. Scale bars represent 100 μm.
(H) Histological scores calculated from (G).
(I) mRNA levels of *Cyp11a1* and *Cyp11b1* quantified by qPCR normalized to *Actb* in colon of DSS-given WT mice that underwent PBS- or TNF- administration.
Data are represented as dotplots with medians unless stated otherwise. Each dot represents one biological replicate.

Table S1. Primers, Related to STAR methods

qPCR Primers			
Target gene	**ENSEMBL gene code**	**Forward sequence**	**Reverse sequence**
Mouse *Gpr35*	ENSMUSG00000026271	Qiagen Cat no: QT00495411	
Mouse *Gapdh*	ENSMUSG00000057666	CATCAAGAAGGTGGTGAAGC	CCTGTTGCTGTAGCCGTATT
Mouse *Actb*	ENSMUSG00000029580	TTCTTTGCAGCTCCTTCGTT	ATGGAGGGGAATACAGCCC
Mouse *Tnf*	ENSMUSG00000024401	CCACCACGCTCTTCTGTCTAC	AGGGTCTGGGCCATAGAACT
Mouse *Il1b*	ENSMUSG00000027398	TGTGAAATGCCACCTTTTGA	GGTCAAAGGTTTGGAAGCAG
Mouse *Il1a*	ENSMUSG00000027399	CGCTTGAGTCGGCAAAGAAAT	CTTCCCGTTGCTTGACGTTG
Mouse *Il23a*	ENSMUSG00000025383	AATGTGCCCCGTATCCAGTG	CAAGCAGAACTGGCTGTTGTC
Mouse *Il10*	ENSMUSG00000016529	ATCGATTTCTCCCCTGTGAA	TGTCAAATTCATTCATGGCCT
Mouse *Il6*	ENSMUSG00000025746	TCGGAGGCTTAATTACACATGTTCT	GCATCATCGTTGTTCATACAATCA
Mouse *Enpp2* (Atx)	ENSMUSG00000022425	GACCCTAAAGCCATTATTGCTAA	GGGAAGGTGCTGTTTCATGT
Mouse *Cyp11a1*	ENSMUSG00000032323	TGGGGTCCTGTTTAAGAGTTCA	CTGCTTGATGCGTCTGTGTAA
Mouse *Cyp11b1*	ENSMUSG00000075604	Qiagen Cat no: QT01198575	
Human *GPR35*	ENSG00000178623	Qiagen Cat no: QT02403128	
Human *GAPDH*	ENSG00000111640	Qiagen Cat no: QT00079247	
Zebrafish *ef1a*	ENSDARG00000020850	ACCTACCCTCCTCTTGGTCG	GGAACGGTGTGATTGAGGGAA
Zebrafish *gpr35a*	ENSDARG00000074633	TTTGAACAGGGCTTTGCGATG	GGTCCATTGGGTTTTGGGAC
Zebrafish *gpr35b*	ENSDARG00000075877	TTGCTCCACACAAACCGTCT	ATATGAACCGGCGTGAAGCA
Zebrafish *il17*	ENSDARG00000041976	CGCCTTGGACATACACAACTT	AGTAAATGGGTTGGGACTCCA
Zebrafish *tnf*	ENSDARG00000009511	GGAGAGTTGCCTTTACCGCT	TTGCCCTGGGTCTTATGGAG
Zebrafish *il1b*	ENSDARG00000098700	ATCAAACCCCAATCCACAGAGT	GGCACTGAAGACACCACGTT
Zebrafish *il22*	ENSDARG00000045673	CGATGACTGATACAGCACGA	TGTGCTCGTCTGATTCCAAG
Zebrafish *il10*	ENSDARG00000078147	TAAAGCACTCCACAACCCCA	GACCCCCTTTTCCTTCATCTTTTC
Zebrafish *enpp2* (Atx)	ENSDARG00000011257	GTGCCGAGGTTTGAGTAG	ACAGTGGTCATCAAAGTCTG
Universal 16S bacterial rRNA	N.A.	ATTACCGCGGCTGCTGGC	ACTCCTACGGGAGGCAGCAGT
Mouse *Gpr35*	ENSMUSG00000026271	ACAAGGCAGGAACTGTG	CCTAGGGCTCAGGCAGC
Genotyping primers			
***Gpr35*-dtTomato**		***Gpr35*-KO**	
GCCTGGATGCCATCTGTTACTACTAC		GCAAGGCCCCAACATCTATAGCTCA	
GATGCAGCCTCTCTAGTCCAACTG		CACTGTCTTTTGTTGCTGCTGCTGT	
GGTCGCTACAGACGTTGTTTGTC		TGGGTTTGGCCCTTAGGATGATGTG	
***Gpr35*-flox**			
GCAAGGCCCCAACATCTATAGCTCA			
CACTGTCTTTTGTTGCTGCTGCTGT			
TGGGTTTGGCCCTTAGGATGATGTG			
GTGGCAGACCATTCCGAAGCTAGAG			

Table S2. Disease Characteristics of Swiss IBD Cohort Study Group Patients Who Provided Biopsies for Expression Analysis, Related to STAR methods

Baseline Group Characteristics				
	Crohn's disease		**Ulcerative colitis**	
	Quiescent (n=20)	**Active (n=11)**	**Quiescent (n=20)**	**Active (n=11)**
Gender (male/female %, n)	60/40 % 12 male, 8 female	36/64 % 4 m, 7 f	35/65% 12 m, 8 f	54/45% 6 m, 5 f
Median age (range), yr	56 (32-81)	39 (31-71)	58 (31-81)	53 (24-68)
Mean BMI (SD), kg/m2	24.15 (Guo et al.)	25.55 (4.9)	24.70 (2.99)	23.89 (4.08)
Median age at diagnosis (range), yr	33.5 (18-60)	21 (14-34)	28.5 (14-65)	30 (16-60)
Median disease duration (range), yr	21.5 (6-45)	19 (7-37)	26 (8-44)	16 (7-38)
CD extent, n (%)				
Ileum isolated	5 (25%)	2 (18%)		
Colon isolated	2 (10%)	3 (27%)		
Ileocolonic	2 (10%)	5 (46%)		
Unknown	11 (55%)	1 (9%)		
UC extent, n (%)				
Proctitis			1 (5%)	1 (10%)
Left-sided colitis			3 (20%)	5 (45%)
Pancolitis			5 (25%)	5 (45%)
Unknown				
Current medical treatment, n (%)				
No treatment	5 (25%)		5 (25%)	1 (9%)
5-ASA	6 (30%)		13 (65%)	9 (81%)
Steroids		6 (54%)		4 (36%)
Immunosuppressants	11 (55%)	1 (9%)	4 (20%)	1 (9%)
Anti-TNF		1 (9%)		3 (27%)
Smoking status				
Non-smoker, n (%)	12 (60%)	6 (54%)	15 (75%)	9 (81%)
Active smoker, n (%)	6 (30%)	5 (46%)	1 (5%)	1 (9.5%)
Unknown	2 (10%)	0	4 (20%)	1 (9.5%)

Table S3. Characteristics of Basel IBD patients Who Provided Biopsies for Immunofluorescence, Related to STAR methods

Patient ID	Gender	Age	BMI	Age at diagnosis	Smoking status	Location inflamed	Location non-inflamed	Treatment at time of study	DAI
Ulcerative colitis									
504	F	50	25.6	34	Unk.	sigma/rectum	trans. colon	none	5
535	F	71	27.3	56	Unk.	rectum/sigmoid	colon	none	6
551	F	53	25	37	Unk.	rectum	Unk.	Unk.	Unk.
619	Unk.	Unk.	Unk.	Unk.	Unk.	sigmoid/rectum	ascend. / trans. colon	None, Salofalk 10 days before	Unk.
Crohn's disease									
558	F	72	19	23	non-smoker	Unk	rectum	Quantalan, Immodium	Unk.
568	M	68	32	52	active	sigmoid	desc. colon	Spiricort, Aldactone, Orfiril	74
620	F	69	21.6	56	active	term. Ileum	ascend. colon	Unk	70

Unk, unknown; DAI, disease activity index

Table S4. Patient characteristics analyzed for the GPR35^{T108M} variant and response to TNF blockers, Related to STAR methods

	Baseline Group characteristics					
	Crohn' disease (n=63)			Ulcerative colitis (n=28)		
	C (n=21)	CT (n=1)	T (n=41)	C(n=9)	CT (n=0)	T (n=16)
Gender, male/female, n (%)	12 (57.14) /9 (42.86)	0 (0) /1 (100)	20 (48.78) /21 (51.22)	6 (66.7) /3 (33.3)	0	10 (62.5) /6 (37.5)
Median age (range), yr	39 (14-63)	54 (54)	38 (17-80)	42 (28-68)	0	36.5 (23-72)
Mean BMI (SD), kg/m^2	22.7 (3.4)	23.5 (.)	23.5 (4.1)	25.7 (1.51)	0	22.6 (5.24)
Median age at diagnosis (range), yr	22 (6-52)	30 (30)	21 (7-51)	25 (15-59)	0	24.5 (15-64)
Median disease duration (range), yr	13 (3-26)	23 (23)	15 (3-41)	13 (9-24)	0	9.5 (4-24)
		CD extent, n (%)				
Ileum isolated	1 (4.76)	0 (0)	4 (9.76)			
Colon isolated	6 (28.57)	0 (0)	9 (21.95)			
Ileocolonic	1 (4.76)	1 (100)	8 (19.51)			
L4	0 (0)	0 (0)	1 (2.44)			
Unknown	11 (52.38)	0 (0)	16 (39)			
		UC extent, n (%)				
Proctitis				1 (11.1)	0	2 (15.4)
Left-sided colitis				4 (44.4)	0	3 (23.1)
Pancolitis				3 (33.3)	0	4 (30.8)
Unknown				1 (11.1)	0	4 (30.8)
		Current medical treatment, n (%)				
No treatment	1 (4.76)	0 (0)	9 (21.95)	1 (11.1)	0	3 (18.75)
5-ASA	2 (9.52)	0 (0)	8 (19.51)	3 (33.3)	0	12 (75)
Steroids	11 (52.38)	0 (0)	10 (24.39)	3 (33.3)	0	5 (31.3)
Immunosuppressants	9 (42.86)	0 (0)	11 (26.83)	3 (33.3)	0	3 (18.75)
Anti-TNF	8 (38.1)	1 (100)	19 (46.34)	1 (11.1)	0	2 (12.5)
Antibiotics	2 (9.52)	0 (0)	1 (2.44)	1 (11.1)	0	0 (0)
Other	9 (42.86)	0 (0)	9 (21.95)	6 (66.6)	0	7 (43.75)
		Smoking status				
Active smoker, n (%)	7 (33.3)	1 (100)	17 (41.46)	1 (11.1)	0	3 (18.8)
Non-smoker, n (%)	13 (61.9)	0 (0)	20 (41.46)	7 (77.8)	0	12 (75)
Unknown	1 (4.76)	0 (0)	4 (9.76)	1 (11.1)	0	1 (6.2)